1-1-2019

Characterization of VPS41 and Its Role in the Regulated Secretory Pathway

Christian Henry Burns
University of Denver

Characterization of VPS41 and its Role in the Regulated Secretory Pathway

---

A Thesis

Presented to

the Faculty of Natural Sciences and Mathematics

University of Denver

In Partial Fulfillment

of the Requirements for Degree

Master of Science

---

by

Christian Henry Burns

June 2019

Advisor: Dr. Cedric S. Asensio

Author: Christian Henry Burns
Title: Characterization of VPS41 and its Role in the Regulated Secretory Pathway
Supervisor: Dr. Cedric S. Asensio
Degree Date: June 2019

ABSTRACT

Insulin secretory granules (SGs) mediate the regulated secretion of insulin, which is essential for glucose homeostasis. The basic machinery responsible for this regulated exocytosis consists of specific membrane proteins present both at the plasma membrane and on insulin SGs. The protein composition of insulin SGs thus dictates their release properties, yet the mechanisms controlling insulin SG formation, which determines this molecular composition, remain poorly understood. VPS41, a component of the endolysosomal tethering HOPS complex, was recently identified as a cytosolic factor involved in the formation of neuroendocrine/neuronal granules. We now find that a stable pool of VPS41 exists outside of HOPS and is required for regulated insulin secretion. Loss of VPS41 leads to a reduction in insulin SG number and changes in their transmembrane protein composition, associated with defects in granule release properties. We further show that a human point mutation, identified in patients with neurological defects but no endocrine defects, enables isolation of the HOPS independent function of VPS41. Finally, we report that mice with a deletion of VPS41 specifically in β-cells develop a diabetic phenotype due to a defect in insulin secretion. Altogether our data suggest that VPS41 contributes significantly to glucose homeostasis.

ACKNOWLEDGEMENTS

I would like to thank Dr. Cedric Asensio for being such a supportive mentor, allowing me the freedom to find this story through the tangled web of potential story-lines. My lab mates without whom this wouldn't have been possible, especially Jenna Triplett for all her late night runs to lab for me. Finally, none of this would have been possible without my family, especially my fiancée Brittaney and all her unwavering support throughout our whole, often crazy, journey together.

TABLE OF CONTENTS

LIST OF FIGURES

INTRODUCTION

Intracellular trafficking to the plasma membrane and extracellular space occurs primarily through a single mechanism of action, the constitutive pathway, by which proteins move from the ER to the Golgi network, bud in vesicles and are delivered to the surface in an unregulated manner (Resa et al, 1987). However, in specialized neuroendocrine cell types, such as neurons and pancreatic β-cells, there exist a second pathway by which they can regulate the intracellular storage and stimulated release of specialized secretory cargo, primarily hormones (**Fig. 1**).

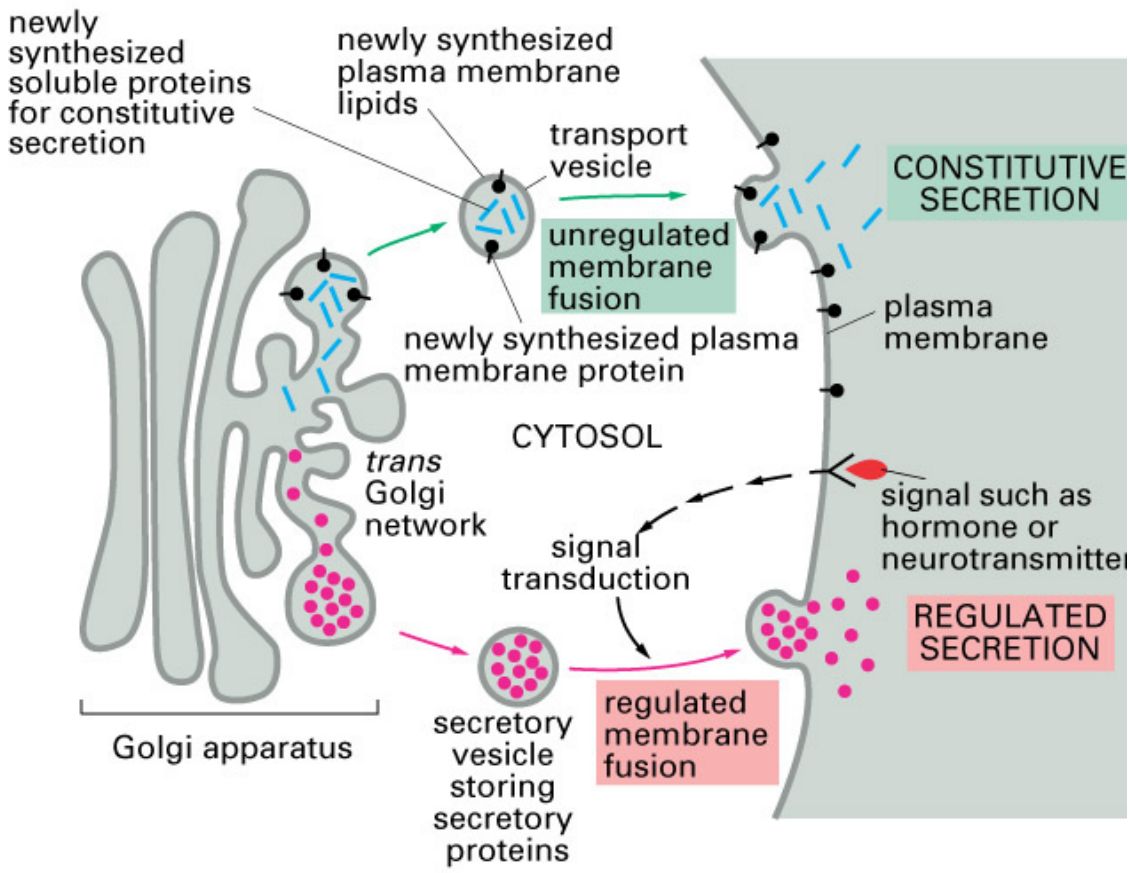

Figure 1: The constitutive and regulated secretory pathways. The constitutive pathway ensures disposal of cellular metabolites as well as delivery of new lipids and proteins to plasma membrane. The regulated secretory pathway take place only in specialized cell types, where dense protein aggregate containing vesicles can be stored intracellularly and released upon exterior cellular stimulus. (Molecular Biology of the Cell. 4th edition. Alberts B, Johnson A, Lewis J, et al. New York; 2002)

These secretory granules (SGs) form at the trans-Golgi network (TGN), where they bud as immature secretory granules, which need further processing to be competent for regulated release (Resa et al, 1987, Tooze, 1998).

These specialized post-Golgi compartments, known as secretory granules (SGs) or large dense-core vesicles (LDCVs), have transmembrane and peripheral membrane cargos that are important for regulating the maturation, transport, and regulated release

(SNARE complexes). SGs also contain a set of soluble protein cargos like peptide hormones, such as insulin, and enzymes that process these hormones into their mature and active form (Tooze 1998). These vesicles then undergo a series of maturation steps, including lumenal acidification, via v-ATPase association, processing and hormone aggregation, which relies on granule acidification, and removal of immature granule markers (e.g., syntaxin 6, vamp4) (Kogel et al, 2010; Sun-Wada et al, 2006; Klumperman et al, 1998; Hinners et al, 2003). Surprisingly, the exact mechanisms dictating SG biogenesis and maturation, which is thought to determine their molecular composition, remains poorly understood. The proper temporal release of these peptide hormones plays a critical role in the body's ability to maintain homeostasis. Pancreatic β-cells, for example, produce insulin and store it within these intracellular SGs. At any given time, these cells can accumulate thousands of insulin SGs, and these vesicles only undergo exocytosis only in response to an extracellular stimulus (e.g., hyperglycemia) (Rorsman et al 2012). The basic machinery responsible for this regulated exocytosis consists of proteins present both at the plasma membrane and on insulin SGs. Thus, the final protein composition of SGs partly dictates their release properties.

Insulin and the counter-regulatory hormone, glucagon, are potent regulators of blood glucose homeostasis. The cells regulating the production and release of these hormones, are found within the islets of the pancreas. Insulin containing SGs are secreted from the β-cells and glucagon from α-cells, which together make up greater than 80% of the total cellular mass of the islet, and these two hormones regulate systemic blood glucose levels within a very narrow window (Roder et al 2016). This preservation of

blood glucose homeostasis is controlled by regulated release of these two hormones, glucagon and insulin, in response to changing blood glucose levels (**Fig 2**). Glucagon is released from α-cells in response to fasting blood glucose, to stimulate gluconeogenesis and downstream increases in blood glucose levels. Insulin, which antagonizes the function of glucagon, is released in response to increased blood glucose levels, such as those that occur post-feeding, and promotes storage of glucose through glycogenesis.

In β-cells the main stimulus for release of insulin, elevated blood glucose, is mediated through uptake of excess glucose from the blood by the GLUT2 glucose transporter. This increased intracellular glucose increases the ATP/ADP ratio in the cell via glycolysis. The increased ATP production leads to closure of ATP-sensitive K+ channels in the cell. K+ build up in the cell, due to inhibited export, induces membrane depolarization and opening of voltage-gated Ca2+ channels, leading to a downstream increase in intracellular Ca2+ concentration, which eventually induces the regulated exocytosis of insulin SGs docked at the plasma membrane (Roder at al, 2016; Henquin, 2000).

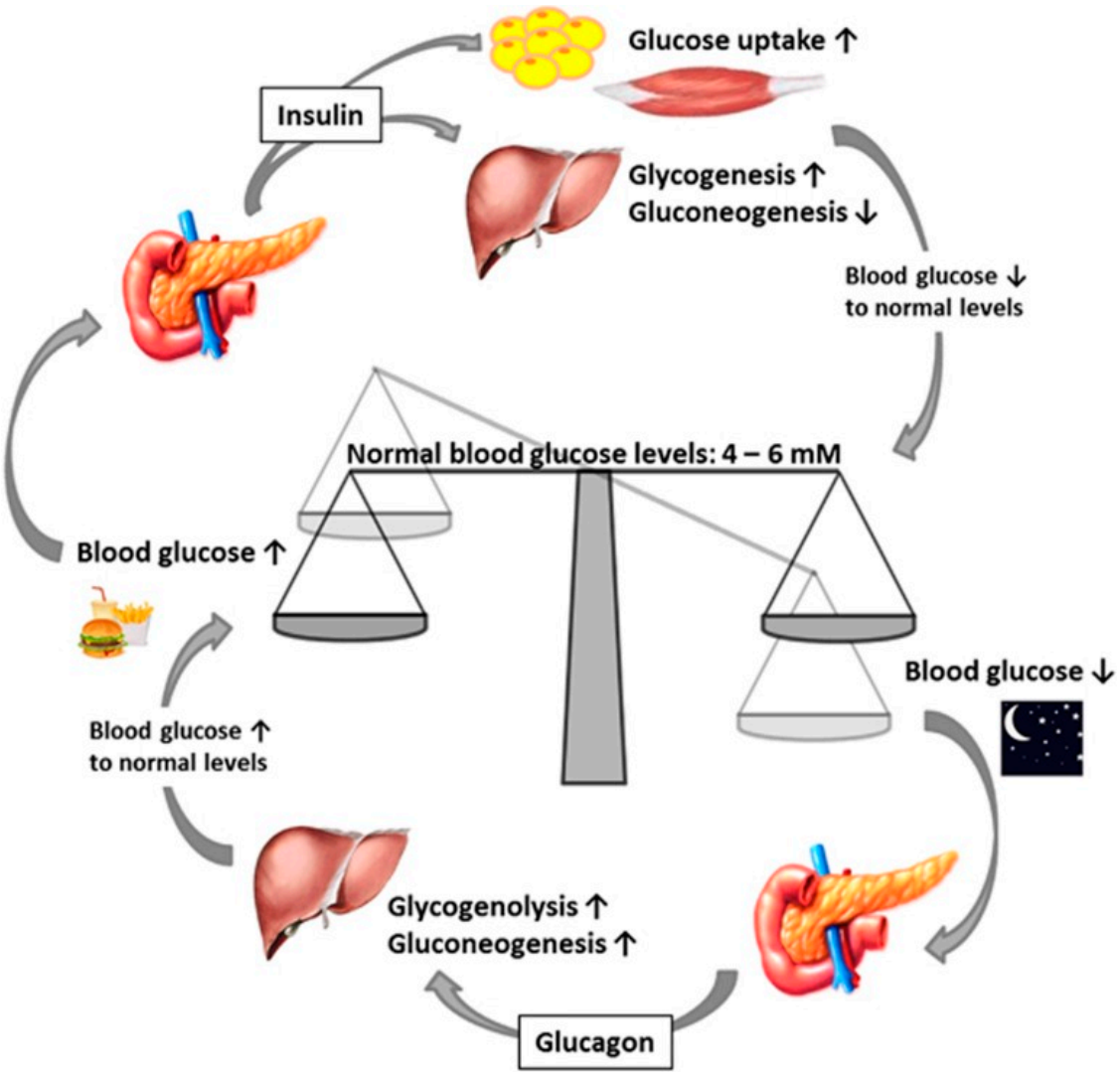

Figure 2: Maintenance pathway of blood glucose levels by insulin and glucagon. Post-feeding blood glucose spikes induce insulin release from pancreatic β-cells, which decreases gluconeogenesis and stimulates glycogenesis in the liver, as well as increasing adipose and muscle glucose uptake to decrease blood glucose levels. Under fasting blood glucose conditions, α-cells increase blood glucose levels by increasing gluconeogenesis and glycogenolysis in liver to increase blood glucose levels (Roder et al 2016).

The regulation of insulin secretion, as well as that of other hormones, needs to be tightly regulated to maintain physiological homeostasis. How these hormone-containing SGs form has long been a topic of debate, currently there exist two major models for the

sorting of cargo leading to the biogenesis of these granules. The "sorting for entry" model, which relies on the idea that sorting of soluble dense core vesicle cargo is mediated by the aggregation of these cargo together in the slightly acidic TGN lumen (**Fig. 3**). This aggregation of cargo leads to the separation of regulated and constitutive cargo into distinct vesicles based solely on the sorting of cargo into these aggregates. This hypothesis is attractive because the identification of sorting receptors in the TGN and uniform sorting signal sequences on soluble cargo has been difficult. "Sorting for entry" is also supported by the aggregation of chromogranin, a regulated secretory cargo, aggregate in conditions similar to the TGN lumen, low pH and calcium (Gerdes et al, 1989), and this has been shown to be sufficient to drive increased sorting and storage of hormones, such as POMC (Natori and Huttner, 1996). However, this model does have its deficiencies. For example, it has been shown that rate of insulin aggregation increases after processing from proinsulin to insulin. There is still significant debate as to when processing of insulin, by the proprotein convertases (PC1/3 and PC2), actually occurs. Localization of the processing of insulin remains unclear, as studies have shown that this process can occur both in the TGN lumen (Xu et al, 1993) as well as post-TGN in immature secretory granules (ISGs)(Orci et al, 1987). This might suggest that insulin can only end up in a mature SG by being retained in a ISG post-TGN budding, which suggests a second model of "sorting by retention". This model proposes that post-TGN compartments are formed that have SG cargo, constitutive cargo, and cargo destined for the lysosome (M6PR for example) and that these cargo are then segregated in post-Golgi

budding events that sort away constitutive and lysosomal cargos into a distinct classes of vesicles, all while the lumen of the vesicle is being acidified and regulated

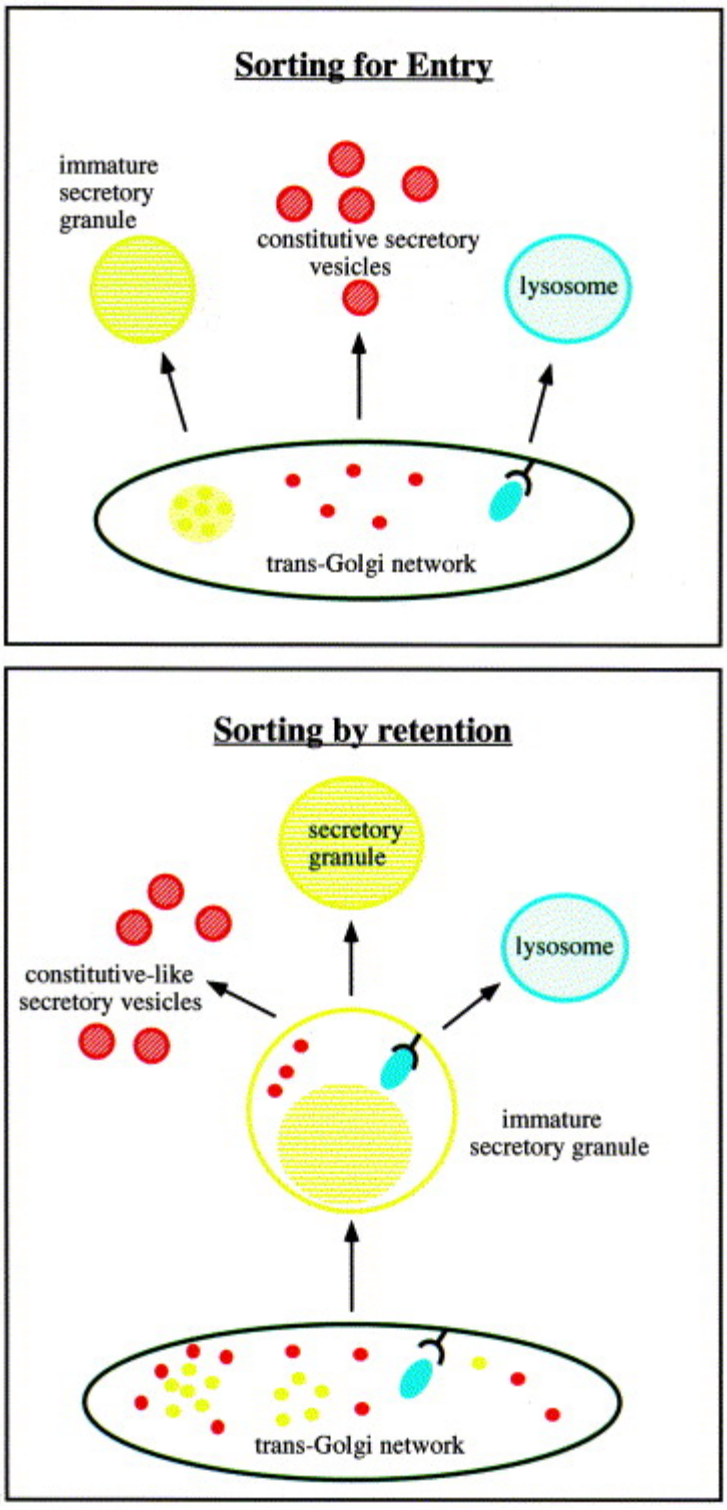

Figure 3: Models of secretory granule biogenesis. "Sorting by entry" model indicates that cargo forms aggregates within the TGN lumen and is separated from constitutive,

unaggregated cargo, by virtue of this aggregation. “Sorting by retention” model suggests that cargo is unaggregated and is budded from the TGN in bulk along with constitutive cargo, which is later budded off into constitutive vesicles as the regulated cargo begins to condense in the acidifying vesicle. (Tooze 1998)

secretory cargo is aggregating to form the well characterized dense-core of a mature secretory granule (Arvan and Castle 1998). There is still a lot that is unknown about how these models might be separate or acting in concert with one another. Additionally, the possibility exists that these models are each true in different cell types dependent on the host of secretory cargo expressed in these cells (Thiele et al, 1997).

However, the biogenesis of secretory granules is not limited to luminal TGN interactions with the secretory cargo itself. Recently, many cytosolic components have been implicated in the formation and maturation of SGs, and that includes BAR domain-containing proteins (Arfaptin-1, Pick1, and ICA69), Rab proteins (Rab-2, Rab-5 and Rab-10), as well as Rab-2 effectors (Ailion et al., 2014; Cao et al., 2013; Edwards et al., 2009; Erlendsson et al., 2014; Gehart et al., 2012; Hannemann et al., 2012; Holst et al., 2013; Pinheiro et al., 2014; Sasidharan et al., 2012; Sumakovic et al., 2009; Hummer et al, 2017). For example, it was recently shown that PICK1, a bar domain containing protein involved in cellular trafficking associates with ISGs and disruption of its function leads to impaired granule storage and morphology in adrenal chromaffin cells without effecting the release properties of the remaining granules (Pinheiro et al, 2014). Disruption of AP3, an adaptor protein involved in trafficking from endosomes and the TGN, also decreases secretory cargo content. AP3 disruption affects the sorting and/or retention of regulated transmembrane secretory cargo (such as VMAT2), which influences their exocytosis

properties (Asensio et al, 2010). Although these factors have been proposed to influence SG formation, their exact mechanism of action remained to be determined. In particular, the spatial-temporal resolution of the cytosolic events controlling sorting, budding and maturation is not well understood.

VPS41/Vam2p and VPS39/Vam6p associate with the VPS Class C core proteins (VPS11, VPS16, VPS18 and VPS33) to form the homotypic fusion and vacuole protein sorting (HOPS) complex, which acts as a tether for mediating heterotypic late endosome-lysosome, and autophagosome-lysosome fusion (Balderhaar and Ungermann, 2013; Nakamura et al, 1997). Disruption in HOPS impairs delivery of endocytic cargo to lysosome and causes defects in autophagosome clearance (Pols et al, 2013; Jiang et al, 2014) (**Fig. 4**). Dysfunction of this pathway has been shown in non-neuroendocrine cell types to be directly responsible for several human diseases, including neurodegeneration, neuron demyelination, blood platelet granule deficiencies, as well as hypopigmentation and vision defects (van der Beek et al, 2019). CORVET, another VPS Class C complex, which mediates the homotypic fusion of early endosomes, shares the sample core complex as HOPS, however VPS41 and VPS39 are replaced with VPS3 and VPS8. VPS3 and VPS8 have been recently shown to be able to interact with each other outside of the CORVET complex and seem to mediate trafficking from early to recycling endosomes (Jonker et al, 2018). This provides reasoning that VPS41 and/or VPS39 may be able to have another function outside of the HOPS complex. Independent of its role in HOPS, VPS41 has also been shown to function in the formation of TGN-derived LAMP-1 post-

Golgi carriers (Pols et al, 2013), which have been shown to carry lysosomal cargos in a M6PR-pathway-independent manner directly from the TGN to the lysosome.

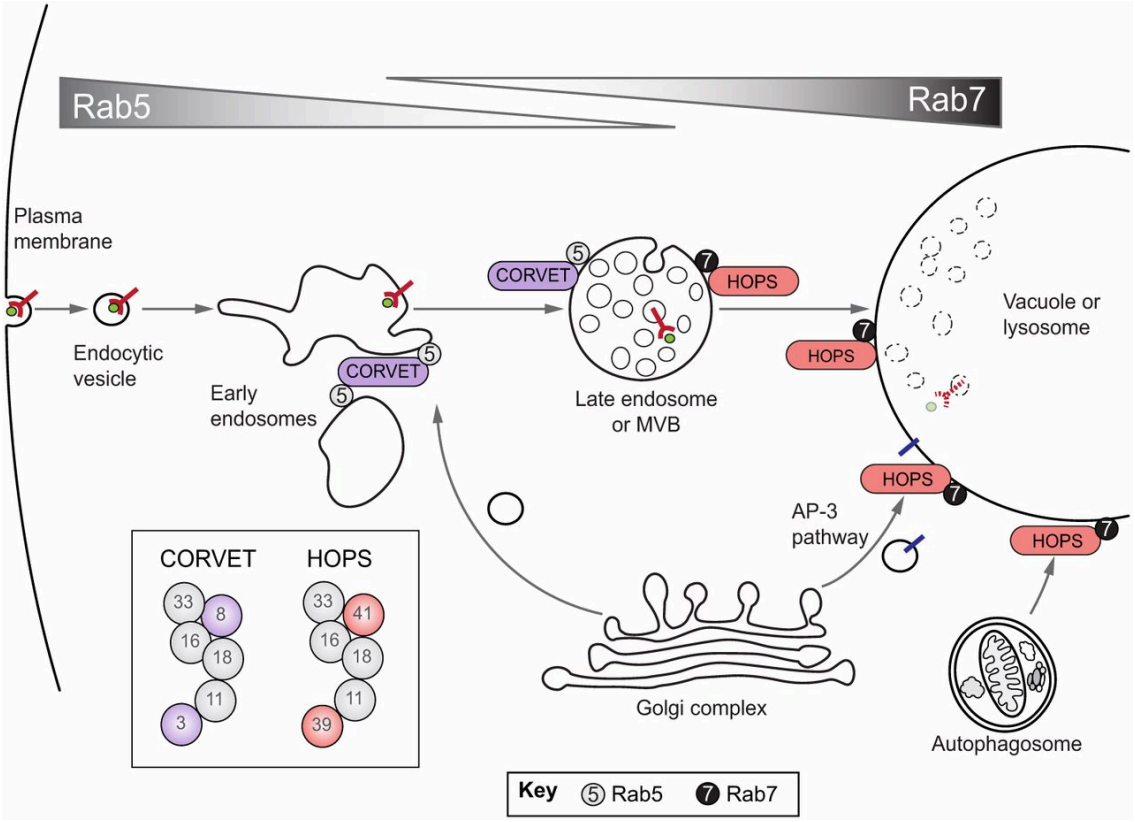

Figure 4: Schematic representation of VPS core complex function within the endolysosomal pathway. HOPS function in fusing late endosomes and autophagosomes with lysosomes is controlled by the association of HOPS with these compartments as they mature, going from Rab5-positive early endosomes to Rab7-late endosome-lysosomal compartments. VPS41-containing HOPS complex interacts directly with Rab7 and other factors on these membranes, to mediate its compartment specificity and regulate the fusion of these specific compartments.

Interestingly, gene expression analysis revealed a significant reduction in VPS41 mRNA levels in islets of a model of mice susceptible to develop diabetes, suggesting that it might be a factor contributing to the development of this pathological condition (Keller

et al, 2008). In accordance with this, it was recently found that VPS41 also affects regulated secretion of peptide hormones and neuropeptides from neuroendocrine cells and neurons, independently of its role in the HOPS complex (Asensio et al, 2013). It was also shown in this study that VPS41 can directly interact with AP3, which also has a role in SG biogenesis (Asensio et al, 2010), as well as itself to form clathrin like structures *in vitro.* This was indicating that VPS41 and AP3 may be acting as the adaptor-coat complex in formation of SGs from the TGN. This was additionally supported by the presence of VPS41 at the trans-Golgi (Pols et al, 2013), and the presence of VPS41 on post-Golgi compartments. Altogether, this led us to hypothesize that VPS41 might be contributing to glucose homeostasis by influencing insulin SG biology. Using siRNA and CRISPR/Cas9 in INS-1 cells, we now show that a stable pool of VPS41 exists outside of the HOPS complex and this pool is required for appropriate insulin storage and secretion. The lack of VPS41 affects SG number, morphology and release properties, by influencing an early step during SG formation. Finally, we report that mice with a deletion of VPS41 specifically in beta-cells are develop a diabetic phenotype due to a defect in insulin secretion.

MATERIALS AND METHODS

Molecular Biology and Plasmids

The human codon-optimized Cas9 and chimeric guide RNA expression plasmid (pX459v2) developed by the Zhang lab (Cong et al., 2013) were obtained from Addgene. To generate gRNA plasmids, a pair of annealed oligos (20 base pairs) were ligated into the single guide RNA scaffold of pX459v2. The following gRNAs sequences were used: Forward (rat): 5′-CACCGACTCTCAGACTGAGCTATGG-3′; Reverse (rat): 5′-AAACCCATAGCTCAGTCTGAGAGTC -3′ to generate the INS1 VPS41 KO line. Rat VPS41 lentiviral plasmid was generated by amplifying VPS41 from rat cDNA using the following primers: WT Forward: 5′-CCTCCATAGAAGACACCGACTCTAGACACCATGGCGGAAGCAGAGGAG-3′; WT Reverse: 5′-TATGGGTAACCCCCAGATCCACCGGTCTTCTTCATCTCCAGGATGGCA-3′. The PCR products were then subcloned by Gibson ligation into pLenti-CMV-GFP-Puro (Addgene #17448). The following primers were used to genotype VPS41 KO INS-1 cells: rVPS41-F: 5′-ATATGGTACCTGCAGAGAGGACTAAACGAGA-3′; rVPS41-R 5′- ATATGAGCTCATGGACGTTGCCATCCAAGT-3′. To test for the presence of indels, the resulting PCR products were ligated into pBlueScript II KS. Isolated plasmids from 10 random colonies were then analyzed for the presence of indels by Sanger -

sequencing. siRNA pools were obtained from Dharmacon (VPS41: 306991, VPS39: 362199) and used as previously described (Asensio et al 2010, 2013).

Cell Culture and Lentiviral Production

INS-1 cells were maintained in RPMI supplemented with 10% FBS, 1mM Na-Pyruvate, 50uM Betamercaptoethanol (BME) under 5% CO_2 at 37°C. INS1 were transfected using Lipofectamine 2000 or Fugene-HD as per manufacturer's instructions. HEK293T cells were maintained in DMEM supplemented with 10% FBS under 5% CO_2 at 37°C. Lentivirus was produced by transfecting HEK293T cells with pLenti-CMV-Puro, psPAX2, and pVSVG using 1mg/mL PEI.

RNA Isolation and qPCR Analysis

RNA was isolated from VPS41 KO or HA-VPS41 INS-1 cells via TriZOL extraction as per manufacturer's instructions (Ambion). Isolated RNA was DNase treated with Turbo DNAse (Ambion). A quantity of 2 μg of total RNA was reverse transcribed with dT(15) oligo (SuperScriptIV, Thermo) and subjected to triplicate qPCR for the target transcripts. qPCR was performed using SYBR Green qPCR Master Mix (BioRad) and a BioRad iQ5 real-time PCR machine (BioRad) with gene-specific primers. The results were normalized to expression of the housekeeping gene ActB. Primers used in this study are detailed in Table A

Name	Sequence	Target
C17-29	CTAGCACCATGAAGATCAAGA	rActB Exon5-6
C17-30	GATCCACATCTGCTGGAAG	rActB Exon5-6
C17-33	CTTTTGTCAAACAGCACCTT	rTubb Exon3-4
C17-34	CAGTGCCAAGGTCTGAAG	rTubb Exon3-4
C19-23	GAACCTGGGACAATGGAC	rINS1/2 Exon1-2
C19-24	TACCGTGAACAAAACTGTCA	rINS1/2 Exon1-2
C19-25	GGTACACTTCCTACAGTGTG	CatB Exon8-10
C19-26	ATGCTTGTATACGCCTGATT	CatB Exon8-10
C19-29	TCCAACTATTCCCTGAAAGC	LAMP1 Exon8-9
C19-30	TCACTTTCTACCCTGAAAGC	LAMP1 Exon8-9

Table A: Primers used for qPCR analysis, primers span exon-intron junctions to ensure that it is reading splice RNA only.

Insulin Secretion Assays

INS-1 insulin secretion was monitored by ELISA (Thermo, ERINS). Cells were plated at 200k cells per 24 well. Prior to stimulation, cells were moved to complete media containing 5mM glucose 18hrs prior, and to KRB buffer supplemented with 1.5mM glucose 2hrs prior and maintained with 5% CO2 at 37°C. Cells were either stimulated in 250ul KRB supplemented with 40mM KCl and 16.7mM glucose or in low glucose KRB for 2hrs. The secreted fraction was removed and spun @1k xg for 5min to remove cellular debris. Cells were lysed in 500ul lysis buffer (50mM TRIS-HCl, 300mM NaCl, 2% v/v TritonX-100) supplemented with 1mM PMSF and 1X protease inhibitor cocktail on ice for 5min. Cellular debris removed by spinning at 21k xg for 10min at 4°C. ELISA was performed as per manufacturer instructions with the secreted fraction being diluted 1:2 and the cellular fraction being diluted 1:10. Proinsulin secretion was monitored by ELISA (Mercodia). Samples, both cellular and secreted, were diluted 1:2 for the assay. Secretion was normalized to cell content by measuring DNA in the cellular fraction. Constitutive secretion from INS-1 VPS41 KO and rescue cells was monitored

via secretion of a secretory pathway targeted GFP (ssGFP). VPS41 KO or HA-VPS41 rescue INS-1 cells were plated in 24 well plate. The next day cells were transfected with ss-pHluorin using Fugene as per manufacturer instructions. 48hrs post-transfection, cells were washed twice with low glucose KRB buffer. Cells were then incubated 3hrs with 250ul of low glucose KRB. After cooling on ice 5min, supernatant containing secreted ss-pHluorin was removed and spun @1k xg for 5min @4C before being transferred to a new tube. Cells were lysed in 250ul lysis buffer and incubated on ice 5min. Cellular debris was removed by spinning lysate @21k xg for 10min. Samples were loaded into black walled 96 well plate (GBO) and fluorescent signal was measure using a plate reader (Tecan) . Blood insulin and islet insulin secretion ELISA was conducted according to manufacturer's protocol (Crystal Chem Ultra Sensitive Mouse ELISA: http://www.crystalchem.com/media/catalog/product/9/0/90080c.pdf)

Immunofluorescence and Spinning Disk Confocal Microscopy

INS-1 cells were rinsed with PBS and fixed in 4% paraformaldehyde in PBS and incubated for 20 min at room temperature. Cells were permeabilized in PBS containing 0.1% Triton X-100 for 10 min at room temperature and blocked in PBS containing 2% BSA, 1% fish skin gelatin, and 0.02% saponin. Primary and secondary antibodies were diluted as reported in Table B. Images were acquired using a custom-built Nikon spinning disk at a resolution of 512 × 512 pixels with a 63× objective (Oil Plan Apo NA 1.49) and an ImageEM X2 EM-CCD camera (Hamamatsu, Japan). Localizations were found using the detection algorithm as previously described (Jaqaman et al, 2008). Localizations were passed to an algorithm that first filtered out spurious noise

with a cutoff of sigma=1.58 pixels (330nm). Distances between both channel's localizations were computed and localizations with a distance d < 1 pixel were deemed colocalized. The relative number of colocalization events versus total localizations for LC3-mCherry+ compartments was computed.

Antibody Target	Source	Dilution (App)
αVPS41 (mouse)	Santa Cruz Biotech. (D-12)	1:100 (Western)
αTubulin (mouse)	DSHB (E-7)	1:500 (Western)
αActin (mouse)	DSHB (JLA20)	1:500 (Western)
αSynaptophysin (mouse)	Synaptic Systems (MMS-618R)	1:2000 (Western)
PC1/3 (rabbit)	Richard Mains (Gift)	1:500 (Western)
αTFE3 (rabbit)	Cell Signaling Tech. (14779)	1:500 (IF)
αCathepsin D (mouse)	Santa Cruz Biotech. (F-12)	1:50 (Western)
αInsulin (mouse)	Sigma Aldrich (K36AC10)	1:1000 (IF)
αHA (rat)	Sigma Aldrich (3F10)	1:1000 (IF)

Table B: Antibodies used in this study, shown with product number and dilution used for specified application.

NPY-pHluorin Exocytosis Imaging

INS-1 cells were co-transfected with NPY-pHluorin and NPY-mCherry. At 1 day after transfection, cells were transferred to poly-l-lysine coated 22 mm glass coverslips. After an additional 2 days, cells were moved to KRB buffer supplemented with 1.5mM glucose 2hr prior to imaging and maintained with 5% CO_2 at 37°C. After reset, cells were washed with KRB buffer and coverslips were transferred to an open imaging chamber (Life Technologies). Cells were imaged close to the coverslips, focusing on the plasma membrane (determined by the presence of NPY-mCherry positive plasma membrane docked-vesicles), using a custom-built Nikon spinning disk at a resolution of 512 × 512

pixels. Images were collected for 100 ms at 10 Hz at room temperature with a 63× objective (Oil Plan Apo NA 1.49) and an ImageEM X2 EM-CCD camera (Hamamatsu, Japan). Following baseline data collection (15 s), an equal volume of 2x KRB buffer containing 114 mM KCl (60mM final) and 32.65mM Glucose (16.7mM final) was added to stimulate secretion and cells were imaged for an additional 45 s. At the end of the experiment, cells were incubated with KRB solution containing 50 mM NH4Cl, pH 7.4, to reveal total fluorescence and to confirm that the imaged cells were indeed transfected. Movies were acquired in MicroManager (UCSF) and exported as tif files. Events were quantified within the first 10s of basal stimulation and between 10s post stimulation (15s after high K+ addition). Event length was calculated based on the time the event remained at or above 20% above baseline signal. For fura imaging, Cells were plated onto poly-l-lysine (Sigma) coated imaging dishes and allowed to adhere in media for 2 days. To load FURA-2, AM (Life Technologies), a basal KRB solution with 500nM FURA was added to the cells. Cells were incubated in the dark at room temperature for 30 minutes, the FURA-2, AM solution was removed and cells washed briefly with basal solution was added to the dish. Cells were imaged using a CoolSNAP HQ2 camera with 6.21 μm/pixel using a 40x oil objective (1.3 N.A.). Images were binned (2x2) and cells were alternatively excited by 340 nm and 380 nm light every 500 ms with a 100 ms interval between exposures. Cells were imaged for 15s under basal conditions prior to perfusing cells with a 90mM K+ KRB solution for 45s.

Density Gradient Fractionation

Equilibrium sedimentation through sucrose was performed as previously described (Asensio et al., 2010, 2013). Briefly, a postnuclear supernatant was prepared from INS-1 cells by homogenization with a ball bearing device (12 μm clearance), loaded onto a 0.6–1.6 M continuous sucrose gradient, and sedimented at 30,000 rpm in an SW41 rotor for 14–16 h at 4°C. Fractions (~750 μl each) were collected from the top and were analyzed by quantitative fluorescence immunoblotting using a FluoChem R imager (ProteinSimple). Insulin concentration in the fractions was determined by ELISA as before, after diluting fraction 1:4 in ELISA lysis buffer for 5min, then diluting sample 1:5 in ELISA diluent.

EGF Degradation Assay

INS-1 cells plated on PLL coated glass coverslips, were washed twice with PBS and starved of serum for 2 h in DMEM with 0.1% BSA (GoldBio). Following starvation, cells were washed twice with ice-cold PBS on ice and incubated with EGF conjugated with Alexa-Fluor 647 (ThermoFisher) at a final concentration of 1 μg/ml for 1 h on ice taking precautions to protect from light. Excess unbound EGF was removed by washing with ice-cold PBS in presence of 0.5% BSA. Cells were chased for indicated times @37C before fixation with 4% PFA in PBS for 30 min on ice. Cells were analyzed by spinning disk confocal microscopy.

Mouse Housing and Breeding

Mice are bred at LAS Facility, Bosch Institute, University of Sydney, Australia and transferred to the Charles Perkins Centre, University of Sydney for experimental procedures. All mice are fed a standard laboratory chow (13% calories from fat, 65% carbohydrate, 22% protein from Gordon's Specialty Stock Feeds, Yanderra, New South Wales, Australia).

Mouse Breeding

VPS41 flox/flox mice x Ins1-Cre mice (https://www.jax.org/strain/026801)
Third generation bred from VPS41 fl/fl x VPS41 fl/-, Ins1-Cre hemi used for experiments

Glucose Tolerance Test

Mice are fasted 5 hours, then analysed prior to IP-GTT by EchoMRI to calculate dose of 2mg/kg glucose to lean mass. Mice are tail tipped for basal blood glucose and insulin measurement, then injected with a 25% glucose solution in injectable water via intraperitoneal route. Blood is collected at 15 minutes for fed insulin measurement, and at the following timepoints: 15, 30, 45, 60, 90, 120, for glucose measurements.

Static Islet Insulin Secretion

Following islet isolation, islets recovered in recovery medium (RPMI, 10% FBS, 11.1mM glucose) for 1hr @ 37C. 10 islets per well (in triplicate) placed into filter unit into KRB with no glucose. Filters with islets transferred to KRB solution containing

2.8mM glucose, as basal incubation, or 16.7mM glucose KRB, as stimulatory. Incubate @ 37C for 20min. Rinse the islets three times with zero glucose KRB. Incubate in low glucose KRB for 1hr. Islets lysed in acid-ethanol (75% ethanol / 1.5% HCl) overnight @ -20C. Secreted and cellular insulin content measured via ELISA.

Fluorescent IHC

Whole pancreas imbedded in paraffin, prior to thin sectioning. Thin section of pancreas are deparaffinized and rehydrated for 3min in following solutions: 2x xylene rinse solution, 1x 50% xylene / 50% ethanol, 1x 100% ethanol, 1x 95% ethanol, 1x 80% ethanol, 1x 75% ethanol, 1x 50% ethanol, 1x ddH_2O**.** Wash slides 3min 2x in PBS with 0.1% BSA, 0.01% NaN_3. Block non-specific antibody association with 2 drops of blocking solution (DAKO). Dilute primary antibody in dilution buffer (DAKO), 100µl per section, and incubate overnight @4C in a humidified chamber. Wash slice 3x with wash buffer for 3min each. Dilute secondary antibody in dilution buffer, 100µl per slice, incubate @RT for 1hr. Rinse with wash buffer 2x for 3min. Rinse with PBS 2x for 3min. Dry slice for 5min @RT. Mount slice with anti-fade DAPI mounting media and a coverslip.

Statistics

Unless indicated otherwise, all statistical analysis was performed using the two-tailed Student's t test. Statistical analyses were conducted using Excel or Prism.

Figure preparation

Images were processed using ImageJ; any changes in brightness and contrast were identical between samples meant for comparison.

RESULTS

The HOPS complex component VPS41 specifically affects regulated insulin secretion in pancreatic β-cells.

In order to assess the potential role of the HOPS complex to insulin secretion, we performed siRNA knock-down (KD) of VPS39 or VPS41 in INS-1 cells. We validated the KD by examining a HOPS specific defect in endo-lysosomal fusion, which results in decreased EGF degradation. Specifically, we incubated our cells with fluorescently labeled EGF and looked at the remaining fluorescence after a 90 min chase. Both VPS39 and VPS41 KD cells exhibited obvious fluorescence retention compared to control cells (**Fig. S1A**), suggesting that the siRNA treatments led to similar HOPS disruption. Surprisingly, analysis of VPS41 levels by western blot revealed that KD of VPS39 also decreased VPS41 protein levels (**Fig. 5A**). To test if this effect was due to instability of HOPS specific components in the absence of full HOPS assembly, we acutely treated VPS39 KD cells with the proteasome inhibitor, MG132, and observed a marked increase in VPS41 levels in presence of the inhibitor (**Fig. S1C-D**). In contrast, the same treatment showed no effect on control cells. These data strongly suggest that a pool of VPS41 normally associated with HOPS becomes susceptible to degradation in the absence of complete HOPS assembly.

We next monitored insulin secretion from these cells via ELISA. We observed a significant decrease in both insulin content and stimulated secretion of insulin in VPS41

KD cells (**Fig. 5B-D**). Importantly, the levels of insulin mRNA determined by real-time qPCR remained unchanged, suggesting that the effect on insulin content is not a consequence of transcriptional changes (**Fig. S1E**). Strikingly, we found that, despite the significant decrease in VPS41 protein levels in VPS39 KD cells, these cells exhibited no defect in regulated insulin secretion. Taken together, we conclude that HOPS specific subunits rely in part on full complex assembly for stability, but that a stable pool of VPS41 can exist outside of HOPS and plays a role in storage and regulated secretion of insulin in β-cells.

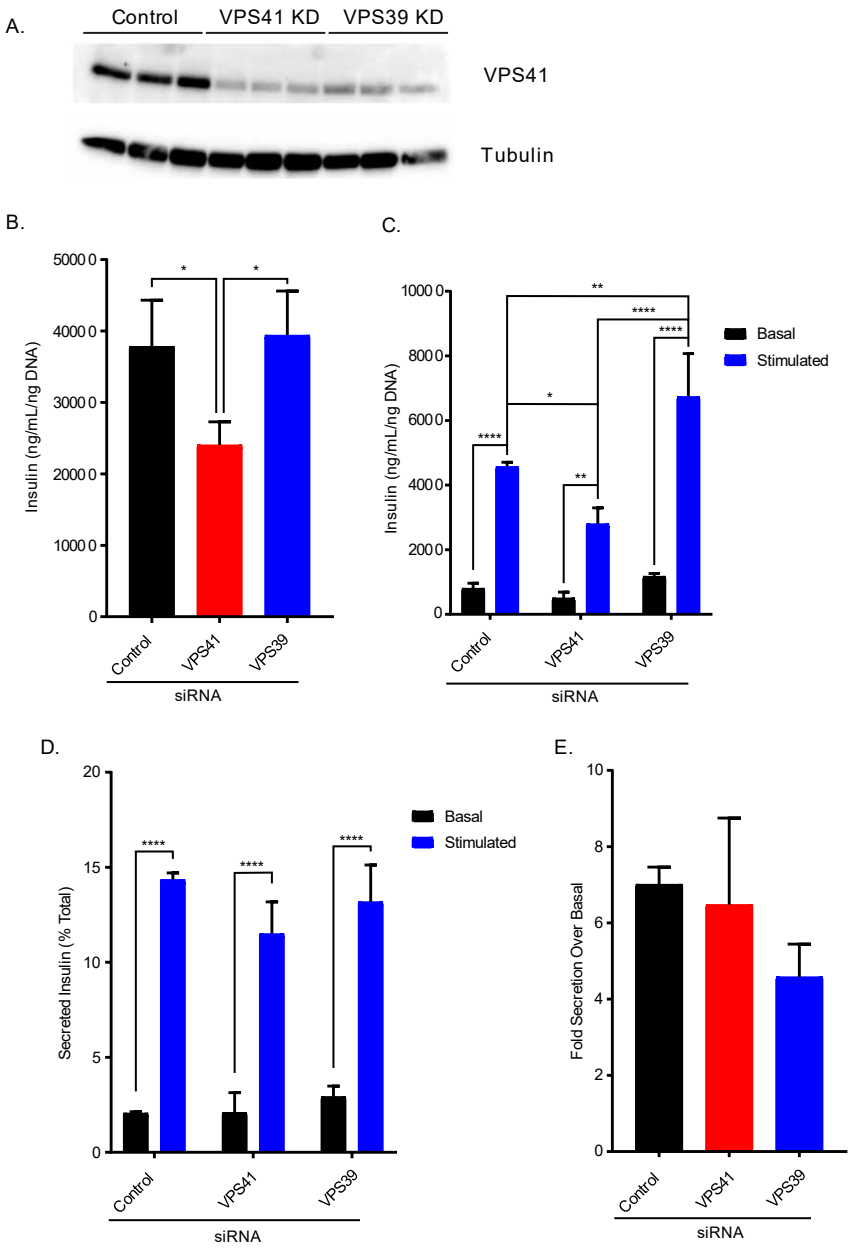

Figure 5: INS-1 cells were transfected with indicated siRNAs. (**A**) Representative western blots showing the levels of VPS41. (**B**) Total cellular insulin levels under basal conditions. (**C**) Basal and stimulated insulin secretion from KO and rescue INS-1. (**D**) Secreted insulin in relation to total cellular content. (**E**) Fold stimulated secretion of insulin. Data indicate mean +/- s.e.m.; n=3 *: $p < 0.05$, **: $p < 0.01$, ****: $p < 0.001$ by one-way ANOVA

Generation of VPS41 KO INS-1 cells

In order to further assess the contribution of VPS41 to insulin secretion, we generated VPS41 KO INS-1 cells using CRISPR/Cas9. The analysis of indels from genomic DNA isolated from these cells revealed the presence of two distinct single base pair insertions predicted to mutate the initiator codon (**Fig. S2A,B**). Consistent with this result, we could not detect VPS41 protein by western blot in lysates generated from these cells, even when using sensitive enhanced chemiluminescent reagents (**Fig. 6A**). As a control for potential Cas9 off-target effects, we generated a rescue line by stably reintroducing full-length VPS41 bearing a N-terminal HA tag (HA-VPS41) using a lentivirus. We confirmed that the expression level matched endogenous levels by western blot and that the expression of HA-VPS41 could indeed be detected in every cells by immunofluorescence against the epitope tag (**Fig. 6A, Fig. S3A**). As expected, these VPS41 KO cells exhibited impaired EGF degradation, consistent with a defect in late endosome/lysosome fusion caused by HOPS deficiency (**Fig. S3B,C**).

VPS41 KO INS-1 cells show a defect in insulin secretion

We next examined basal and stimulated insulin secretion from KO and rescue cells by ELISA and, consistent with the siRNA experiments, observed that lack of VPS41 led to a significant decrease in stimulated insulin secretion as well as a substantial reduction in cellular insulin stores (**Fig. 6B,C**). Importantly, we still observed a defect in insulin secretion after normalizing secreted values to cellular stores (**Fig. 6D**) leading to a decrease in the fold stimulation over basal (**Fig. 6E**). Consistent with the ELISA results, we also

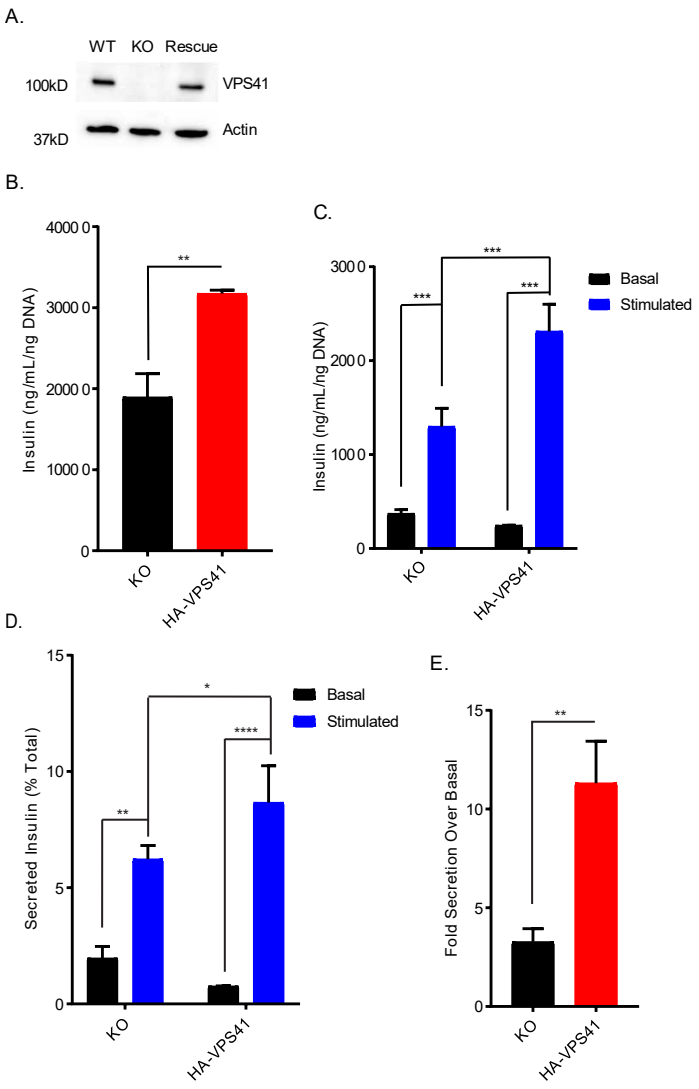

Figure 6: (**A**) Representative western blots showing the levels of VPS41 in WT, VPS41 KO, and HA-VPS41 rescue INS-1 cells. (**B**) Total cellular insulin levels under basal conditions. (**C**) Basal and stimulated insulin secretion from KO and rescue INS-1. (**D**) Insulin secretion relative to cellular insulin stores. (**E**) Fold stimulated insulin secretion over basal insulin secretion. Data indicate mean +/- s.e.m.; n=3 *: $p < 0.05$, **: $p < 0.01$,***: $p < 0.001$, ****: $p < 0.0001$ by one-way ANOVA

observed a decrease in total insulin signal in VPS41 KO cells by immunofluorescence, mostly due to peripheral depletion leading to a relative increase in perinuclear signal (**Fig. S4A-C**). As the insulin ELISA kit can also recognize proinsulin to some extent, we separately measured proinsulin levels in secreted and cellular fractions. VPS41 KO cells displayed slightly increased cellular stores of proinsulin (**Fig. S5A**). As a consequence, these cells show an increase in the ratio of cellular proinsulin over insulin (**Fig. S5B**). However, VPS41 KO cells showed no difference in proinsulin secretion (**Fig. S5C-E**). We conclude that VPS41 regulates insulin content and is required for the regulated release of insulin.

The absence of VPS41 leads to changes in SG number and biochemical and morphological properties

These results prompted us to further determine the biochemical properties of SGs in absence of VPS41. For this, we relied on equilibrium sedimentation through sucrose and determined insulin distribution within the gradient by ELISA. In VPS41 KO cells, insulin shifted to lighter fractions compared to rescue cells (**Fig. 7A,B**). To confirm that insulin containing fractions were in fact SGs, we determined the localization of an additional SG cargo, proprotein convertase 1/3 (PC1/3), by western blot and found that it co-sedimented with insulin in both VPS41 KO and rescue cells. Additionally, this effect appears to be specific to SGs, as synaptophysin (p38) sedimentation remained unaffected. Analysis of thin-sections by EM revealed that the absence of VPS41 decreases the number of SGs (**Fig 7C**). Altogether these data suggest that the absence of VPS41 affects the number and.

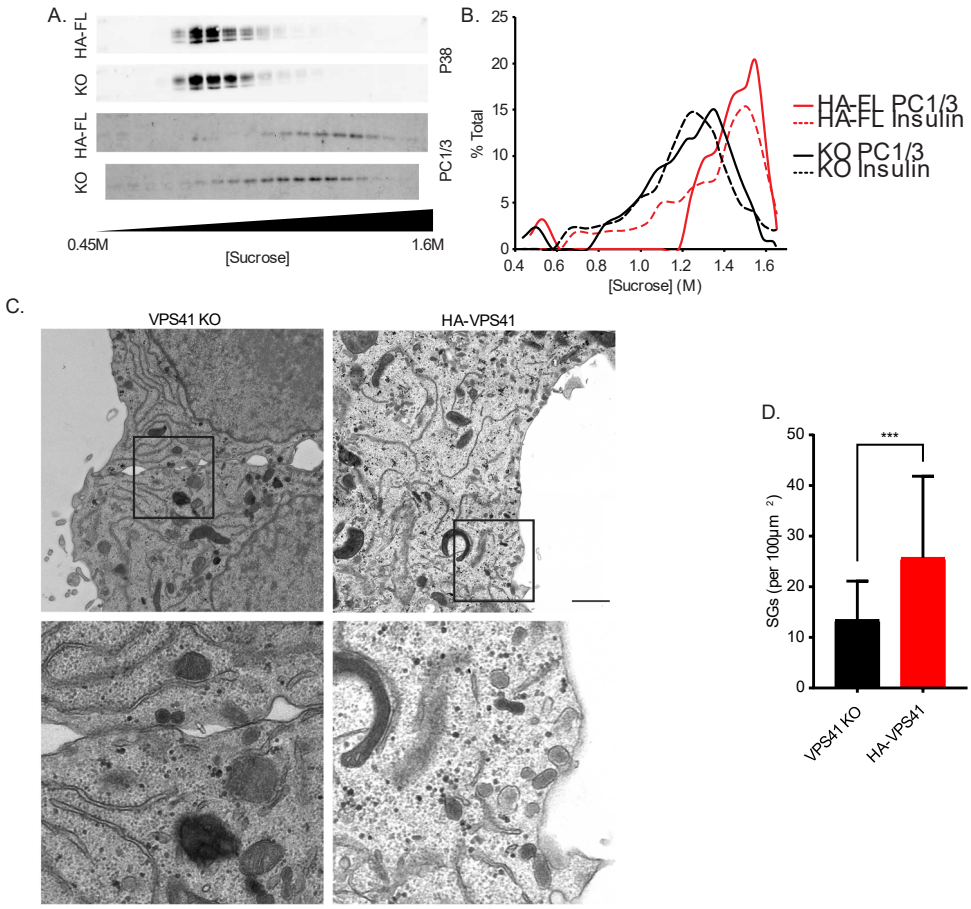

Figure 7: Postnuclear supernatants (PNS) obtained from VPS41 KO and HA-VPS41 rescue INS-1 cells were separated by equilibrium sedimentation through 0.6–1.6 M sucrose. Fractions were collected from the top of the gradient and assayed for (**A**) synaptophysin (p38) and proprotein convertase 1/3 (PC1/3) by quantitative fluorescence immunoblotting. The graphs (**B**) quantify the immunoreactivity in each fraction as a percentage of total gradient immunoreactivity from one experiment. Insulin levels for the same fractions were determined by ELISA. Similar results were obtained in an additional independent experiment. (**C**) Representative thin section EM images of VPS41 KO and HA-VPS41 INS-1 cells. Scale bar indicates 1 µm. (**D**) Quantification of total SGs per cell normalized to the area of the section. Data indicate mean +/- s.e.m.; n= 45 cells for KO and 18 cells for HA-VPS41 ***: $p < 0.001$

biochemical properties of insulin SGs, suggesting that VPS41 might be required for more than one aspect of their biogenesis

The absence of VPS41 leads to lysosome and autophagosome biogenesis, but does not lead to increased insulin degradation

How does VPS41 influence insulin cellular stores? Lack of VPS41 could influence insulin turnover. Interestingly, the lysosomal mTOR complex (mTORC) regulates the levels of lysosomal and autophagosomal gene products (Puertollano 2014)). Specifically, inactivation of mTORC in response to cellular starvation leads to nuclear translocation of the transcription factor TFE-3, which directly activates lysosomal and autophagosomal gene expression. Interestingly, it was recently observed that loss of VPS41 in HeLa cells leads to a striking increase in lysosomal biogenesis (van der Welle et al, unpublished), indicating that defects in endolysosomal degradation due to HOPS deficiency mimic cellular starvation by activating TFE-3. We immunostained VPS41 KO and rescue INS-1 cells for TFE-3 and indeed observed an increase in constitutive nuclear localization of this transcription factor under non-starving conditions (**Fig. 8A,B**). Consistent with this, we detected an increase in the expression levels of lysosomal genes (lamp-1, cathepsin B) by real-time qPCR and by western blot (**Fig. S6A-C**). We also quantified the number of active lysosomes using Magic Red (MR), a membrane-permeable dye that becomes fluorescent after cathepsin B activation, and found a significant increase in active lysosomal compartments in absence of VPS41 (**Fig. 8C,D**). We next tested whether this increase in lysosomal biogenesis could contribute to the

decrease in insulin content observed in absence of VPS41. However, we found that treatment with lysosomal hydrolase inhibitors for 24h had no effect on insulin content (**Fig. 8E**). Thus, although the lack of VPS41 triggers a response aiming at increasing lysosomal biogenesis, it does not lead to insulin degradation. In addition, we found that mature cathepsin D redistributed to lighter fractions in VPS41 KO cells by equilibrium sedimentation through sucrose (**Fig 8F**), suggesting differences in biochemical properties of these lysosomes, probably due to diminished flux of endocytic cargo.

HOPS deficiency also leads to an accumulation of autophagosomes (Jiang et al 2014). To test whether this phenomenon holds true in INS-1 cells, we transfected VPS41 KO and rescue cells with LC3-eGFP and indeed found a striking increase in the number of LC3 positive compartments in VPS41 KO cells (**Fig. 8G,H**). However, we found a significant decrease in autophagic flux using a two color mCherry-eGFP-LC3B reporter (N'Diaye et al 2009) (**Fig 8I,J**). In addition, insulin did not colocalize with these stalled autophagosomes by immunofluorescence and by immuno-EM in the KO (**Fig S6D**). It is thus unlikely that a significant portion of insulin SGs gets engulfed into autophagic structures in absence of VPS41. Altogether these data indicate that the lack of VPS41 does not lead to missorting of insulin to autophagosomes or lysosomes.

VPS41 KO cells display normal TGN budding kinetics, but show missorting of transmembrane proteins leading to constitutive insulin secretion

We next tested whether the decrease in SG number observed in VPS41 KO cells could be a consequence of a budding defect from the TGN. For this, we relied on the RUSH system (Boncompain et al 2012) using a ER hook and biotin to release a

synchronized wave of SG cargo (NPY-GFP). Using live-imaging, we monitored the movement of NPY-GFP along the secretory pathway (Maslar et al, unpublished). Upon addition of biotin, NPY-GFP trafficked from the ER to the Golgi, followed by its incorporation into post-Golgi carriers in VPS41 KO and rescue cells. By measuring changes in fluorescence, we determined TGN exit rates and found that they remained unchanged between the two cell lines (**Fig. 9A**). These data suggest that the budding kinetics of soluble SG cargoes remain unaffected.

After ruling out insulin degradation and budding defects as an explanation for the decrease in insulin content, we reasoned that the absence of VPS41 could lead to the formation of "malfunctioning" SGs, which are undergoing exocytosis constitutively and thus are not accumulating intracellularly. Interestingly, although we did not observe a statistical difference in basal insulin secretion when analyzed by ANOVA together with stimulated secretion data, VPS41 KO INS-1 cells exhibit a 50% increase in basal secretion compared to rescue cells, and this effect is significant by t-test ($p = 0.0067$) when compared directly. (**Fig. 6B**). We next looked at the behavior of a transmembrane SG marker (phogrin) using RUSH (Maslar et al, unpublished) and observed a striking decrease in its colocalization with insulin after biotin addition in VPS41 KO cells. (**Fig 9B,C**) This suggests that the absence of VPS41 affects SG protein composition, in particular transmembrane proteins and this change might affect the ability of SGs to accumulate intracellularly.

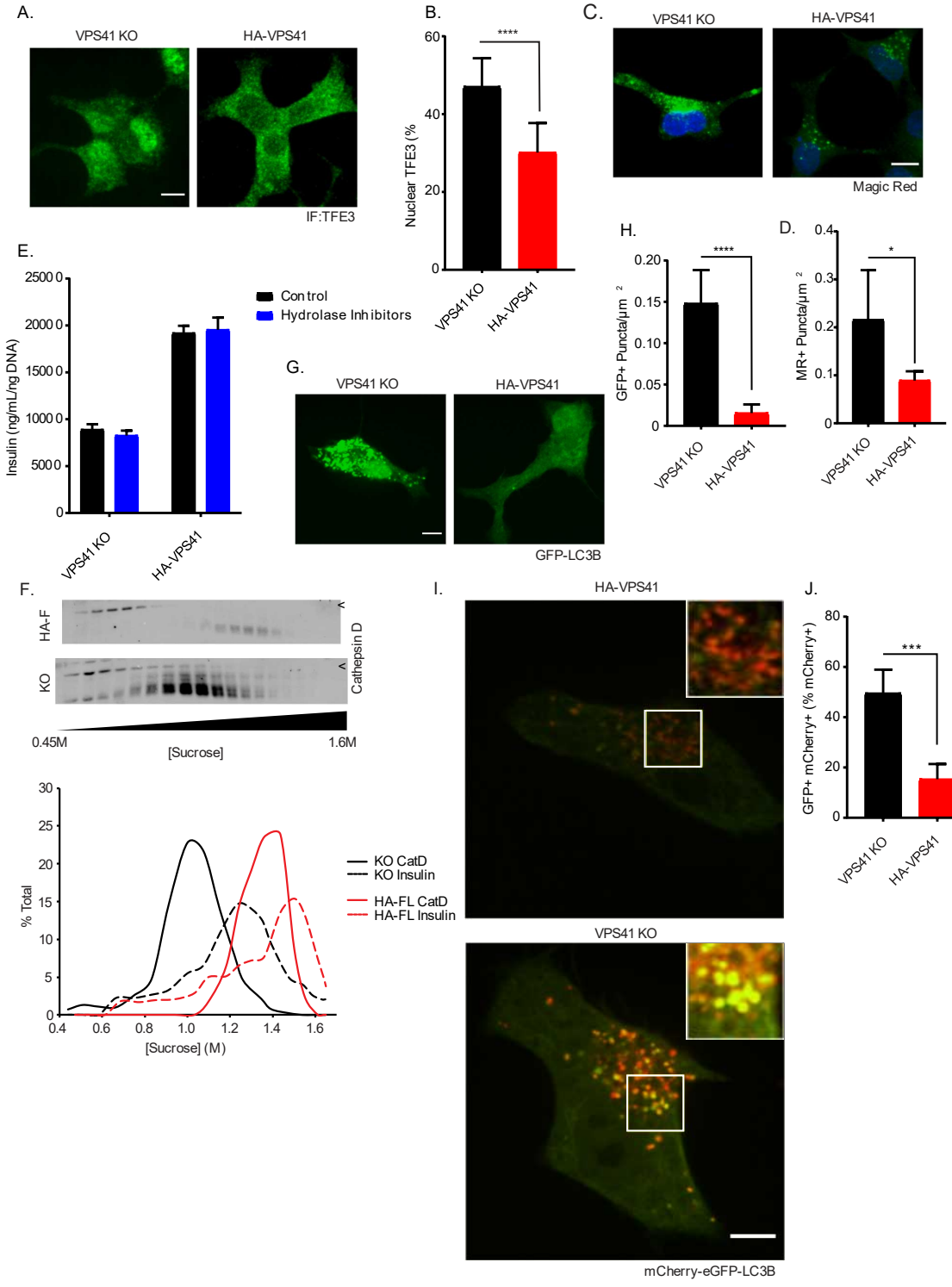
A.
VPS41 KO
HA-VPS41
IF:TFE3
B.
****
Nuclear TFE3 (%
60
40
20
0
VPS41 KO
HA-VPS41
C.
VPS41 KO
HA-VPS41
Magic Red
H.
****
GFP+ Puncta/µm 2
0.20
0.15
0.10
0.05
0
VPS41 KO
HA-VPS41
D.
*
MR+ Puncta/µm 2
0.4
0.3
0.2
0.1
0
VPS41 KO
HA-VPS41
E.
Insulin (ng/mL/ng DNA)
2500 0
2000 0
1500 0
1000 0
5000
0
Control
Hydrolase Inhibitors
VPS41 KO
HA-VPS41
G.
VPS41 KO
HA-VPS41
GFP-LC3B
F.
HA-F
KO
Cathepsin D
0.45M
1.6M
[Sucrose]
% Total
30
25
20
15
10
5
0
0.4
0.6
0.8
1.0
1.2
1.4
1.6
[Sucrose] (M)
KO CatD
KO Insulin
HA-FL CatD
HA-FL Insulin
I.
HA-VPS41
VPS41 KO
mCherry-eGFP-LC3B
J.
***
GFP+ mCherry+ (% mCherry+)
80
60
40
20
0
VPS41 KO
HA-VPS41

Figure 8: (**A**) Representative images of TFE-3 immunostaining in VPS41 KO and HA-VPS41 rescue INS-1 cells imaged by spinning disk confocal microscopy. (**B**) Quantification of the amount of total TFE3 within the nuclear compartment, as determined by DAPI staining. (**C**) VPS41 KO and rescue cells were exposed to the Cathepsin B cleavable dye, Magic Red, and imaged using a spinning disk confocal microscope. (**D**) Quantification of Cathepsin B Magic Red positive compartments. (**E**) Insulin levels were determined by ELISA from cell lysates incubated with hydrolase inhibitors. (**F**) PNS were separated by equilibrium sedimentation through 0.6–1.6 M sucrose. Fractions as described in Figure 3 and assayed for Cathepsin D (CatD). The graphs quantify the immunoreactivity in each fraction as a percentage of total gradient immunoreactivity from one experiment. Similar results were observed in an additional independent experiment. Insulin values from Figure 3 are shown as a reference. Cells transfected with LC3B-eGFP (**G**) or mCherry-eGFP-LC3B (**I**) were imaged for presence of LC3+ puncta. (**H**) Quantification of LC3-GFP + puncta in KO and rescue cells. (**J**) Percentage of of mCherry-LC3 positive puncta that also have unquenched GFP-LC3. Data indicate mean +/- s.e.m.; n=3 for LC3-GFP, n=3 for MR and n=3 for 2 color LC3 *: $p < 0.05$, ***: $p < 0.001$, ****: $p < 0.0001$. Scale bars: 10μm

Loss of VPS41 leads to a defect in insulin granule exocytosis

These data indicate that lack of VPS41 might affect SG release properties. To test whether the absence of VPS41 leads to an impairment in SG exocytosis, we transfected VPS41 KO and rescue cells with NPY-pHluorin and monitored exocytosis in real-time using spinning-disk confocal microscopy. Under basal conditions, we observed very few exocytosis events across the two cell lines, confirming that NPY-pHluorin does not mis-sort to the constitutive secretory pathway in absence of VPS41. However, under stimulatory conditions, HA-VPS41 rescue cells showed a robust increase in the number of events (61 events/μm/sec ($x10^{-4}$)), but this number was dramatically reduced in the KO cells (12 events/μm/sec ($x10^{-4}$)) (**Fig. 9D**). Interestingly, we also found that the type of events remaining in the KO cells exhibited very different kinetics. Indeed, in rescue cells, the large majority of events (>80%) lasted less than 1s, but in the KO cells, 50% of

events went on for more than 1s, with some lasting up to 9s (**Fig. 9E**). Importantly, this exocytosis defect could not be explained by an impairment in the excitability of the cells as calcium imaging experiments revealed that VPS41 KO and rescue cells displayed similar responses following depolarization (**Fig. 9F**). In order to examine if these effects on stimulated exocytosis are evident directly after budding, we relied again on the RUSH system to look at NPY-pHluorin release properties at different times (2, 3, or 4h) after biotin addition. We observed a striking reduction in the number of events at each time point, but the defect tended to become more pronounced with time (**Fig 9G,I**). Interestingly, the effect on kinetics of exocytosis remained unchanged at 2h and became apparent only at later time points (**Fig 9H,J**). Altogether, these data suggest that the absence of VPS41 reduces the total number of SGs that are available for release and that the few SGs competent for release tend to change their exocytosis kinetics after budding.

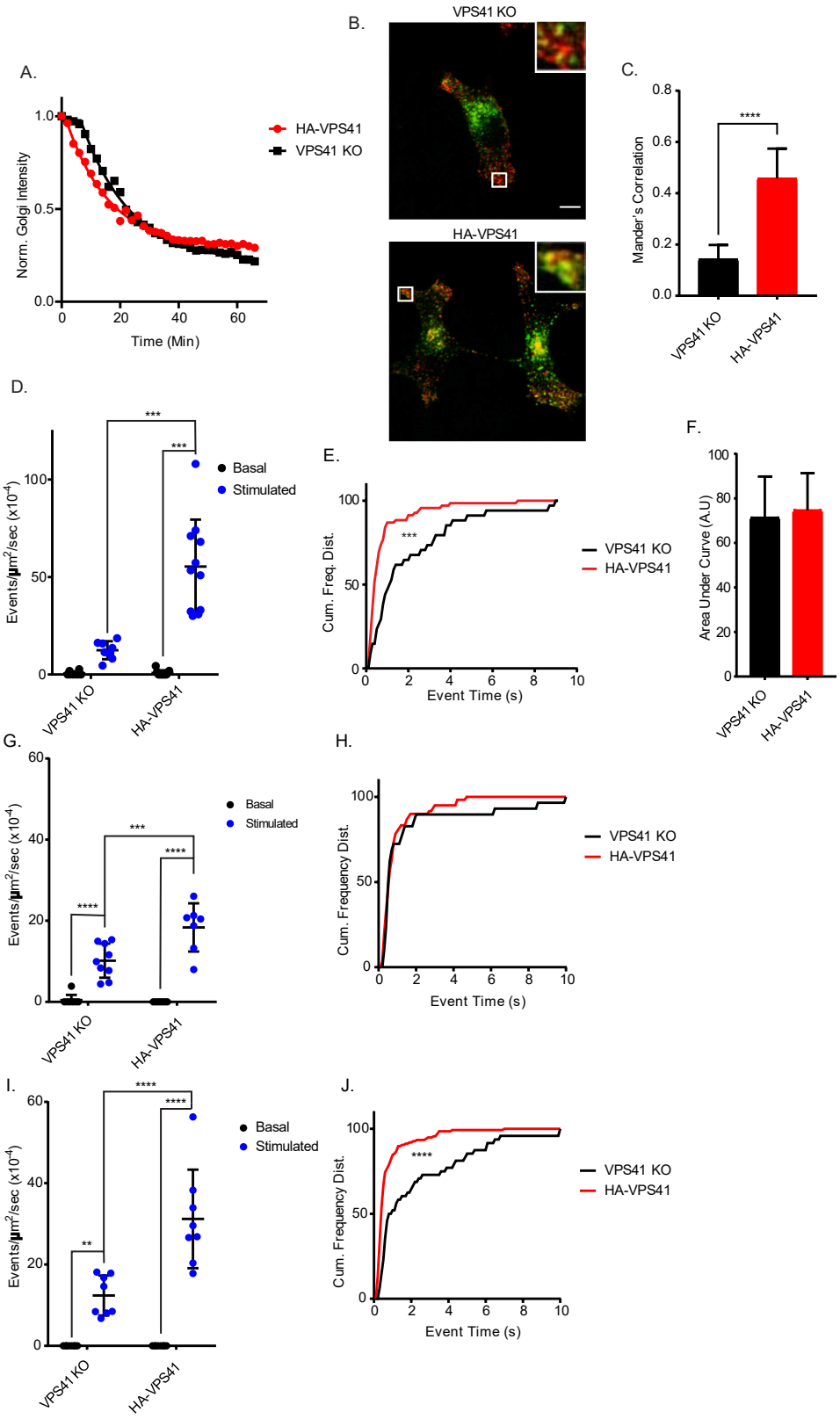
A.
Norm. Golgi Intensity
Time (Min)
HA-VPS41
VPS41 KO
B.
VPS41 KO
HA-VPS41
C.
Mander's Correlation
****
VPS41 KO
HA-VPS41
D.
Events/μm²/sec (x10⁻⁴)
***
***
Basal
Stimulated
VPS41 KO
HA-VPS41
E.
Cum. Freq. Dist.
***
Event Time (s)
VPS41 KO
HA-VPS41
F.
Area Under Curve (A.U)
VPS41 KO
HA-VPS41
G.
Events/μm²/sec (x10⁻⁴)
***
****
****
Basal
Stimulated
VPS41 KO
HA-VPS41
H.
Cum. Frequency Dist.
Event Time (s)
VPS41 KO
HA-VPS41
I.
Events/μm²/sec (x10⁻⁴)
****
****
**
Basal
Stimulated
VPS41 KO
HA-VPS41
J.
Cum. Frequency Dist.
****
Event Time (s)
VPS41 KO
HA-VPS41

Figure 9: (**A**) Representative Golgi decay curves of exit of NPY-eGFP from VPS41 KO and HA-VPS41 INS-1 after induction of cargo wave via biotin addition. (**B**) Representative images of Phogrin-eGFP co-stained with insulin 24hrs post-biotin addition, Scale bars: 10μm. (**C**) Manders colocalization coefficent of phogrin colocalization with insulin signal in VPS41 KO and rescue (**D**) Quantification of NPY-pHluorin exocytosis events in VPS41 KO and HA-VPS41 rescue INS-1 cells over a 10s basal or stimulated period. (**E**) Cumulative frequency distribution of NPY-pHluorin exocytosis event duration in VPS41 KO and rescue cells. (**F**) Quantification of calcium imaging (Fura) in response to depolarization (high K^+) in KO and rescue cells. (**G**) Quantification of NPY-pHluorin exocytosis events in VPS41 KO and HA-VPS41 rescue INS-1 cells over a 10s basal or stimulated period 2hrs post-biotin addition. (**H**) Cumulative frequency distribution of NPY-pHluorin exocytosis event duration in VPS41 KO and rescue cells 2hrs post-biotin addition. (**I**) Quantification of NPY-pHluorin exocytosis events in VPS41 KO and HA-VPS41 rescue INS-1 cells over a 10s basal or stimulated period 3hrs post-biotin addition. (**J**) Cumulative frequency distribution of NPY-pHluorin exocytosis event duration in VPS41 KO and rescue cells. .Data indicate mean +/- s.e.m.; n=3 *: ***: $p < 0.001$, ****: $p < 0.0001$ Event number analyzed by one-way ANOVA. Event duration analyzed by Kolmogorov Smirnov.

Human point mutation S285P rescues insulin secretion but not HOPS

Human patients carrying a point mutation within VPS41 (S285P) exhibit neurological defects without any known endocrine dysregulation (van der Welle et al, unpublished). We reasoned that this point mutant could help distinguish between HOPS dependent and independent effects of VPS41. Thus, we stably expressed an HA tagged rat VPS41^{S284P} (S285P equivalent) in VPS41 KO INS-1 cells and found that they displayed a defect in EGF degradation and LC3 puncta accumulation similar to VPS41 KO cells (**Fig 10A, S8A**) (**Fig S8 B,C**), indicating a defect in HOPS. We next monitored insulin secretion from these cells and observed that this mutant completely rescues insulin secretion and storage (**Fig. 10B-E**). These data suggest that this mutation enables VPS41 to function independently of HOPS only.

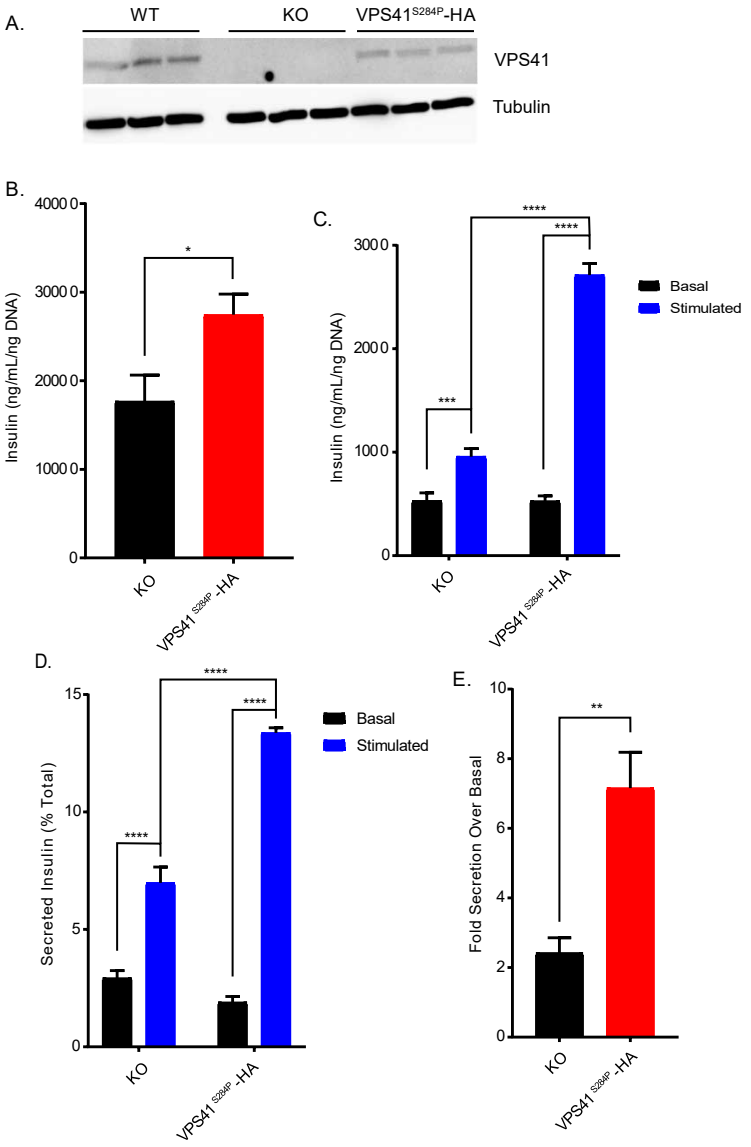

Figure 10: (**A**) Representative western blot showing VPS41 levels in WT, KO and KO expression of VPS41^{S284P}-HA variant. (**B**) Total cellular insulin levels under basal conditions. (**C**) Basal and stimulated insulin secretion from KO and rescue INS-1. (**D**) Insulin secretion relative to cellular insulin stores. (**E**) Fold stimulated insulin secretion over basal insulin secretion. Data indicate mean +/- s.e.m.; n=3 *: $p < 0.05$, **: $p < 0.01$, ***: $p < 0.001$, ****: $p < 0.0001$ by one-way ANOVA

Mice with beta-cell specific deletion of VPS41 show a defect in insulin secretion

To explore the physiological role and significance of VPS41 in glucose homeostasis, we deleted VPS41 specifically in beta-cells of the pancreas by crossing mVam2 fl/fl animals with mice expressing Cre under the control of the insulin promoter (Aoyama et al 2012, Thorens et al 2015). Comparison of VPS41 protein levels in lysates prepared from isolated islets revealed a ~75% reduction in VPS41 KO mice (**Fig S9 A-C**). Importantly, VPS41 levels remained unchanged in whole brain, hypothalamus and liver lysates, indicating that the deletion is specific (**Fig S9A,B**). VPS41 KO mice did not show any changes in body weight, fat or lean mass at 8 or 15 weeks (**Fig. 11A, Fig. S10A**), but these animals exhibited a dramatically higher fasting glycemia (~25mM) compared to age-matched controls (~10mM) (**Fig. 11B, Fig S10B**). We next performed a glucose tolerance test (GTT) on 8 weeks old animals and found that VPS41 KO mice are massively glucose intolerant (**Fig. 11C**). Additionally, we also observed a pronounced reduction in basal and glucose stimulated plasma insulin levels during GTT (**Fig. 11D**). At 15 weeks, VPS41 KO mice displayed an even more severe phenotype (**Fig. S10C,D**). Staining of whole pancreas sections by immunofluorescence revealed a significant reduction in insulin levels, but no apparent change in glucagon levels (**Fig. 12A**). Finally, we isolated islets from 15 week old animals and determined insulin secretion in vitro. Consistent with our data in INS-1 cells, we observed a dramatic defect in basal and glucose stimulated secretion from isolated islets (**Fig. 12B, D**), together with a reduction in insulin content (**Fig. 12C**).

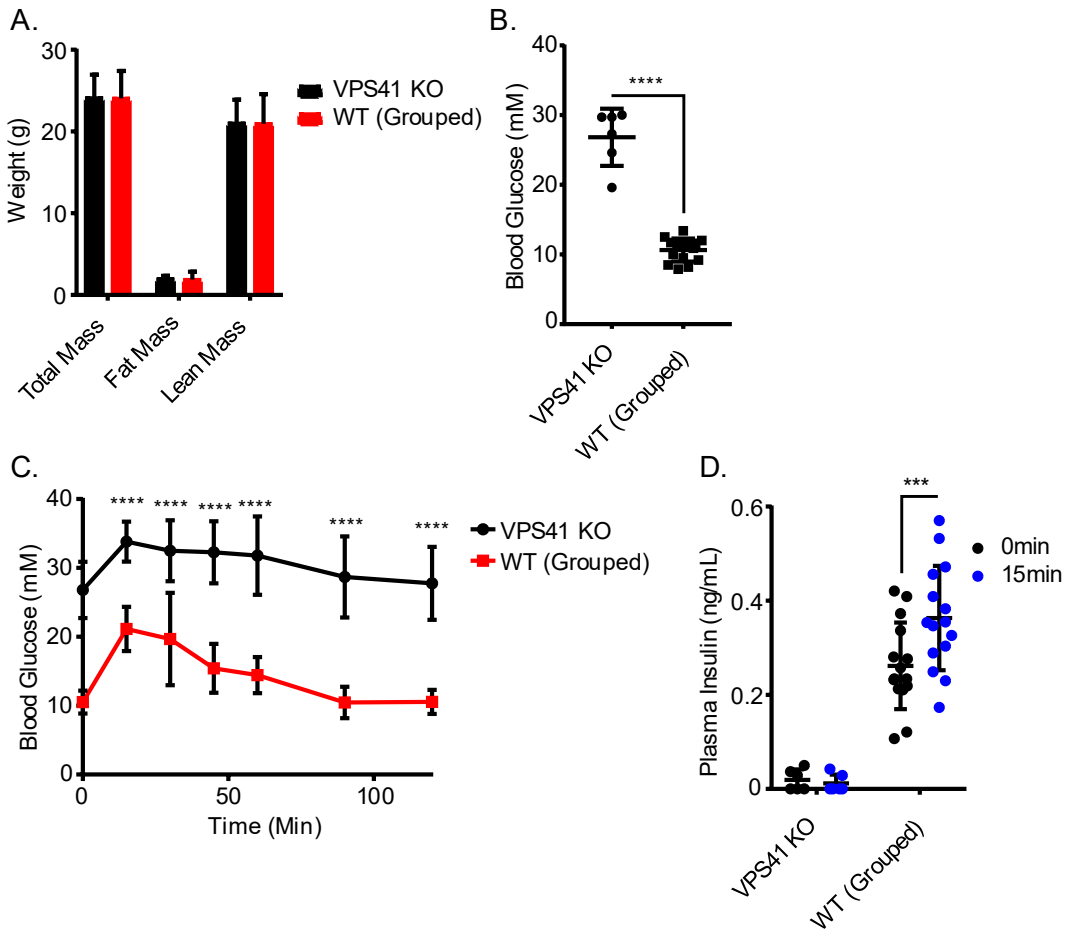

Figure 11: (**A**) Fat and lean mass measurements of age matched 8 week old WT and VPS41 KO mice. (**B**) Blood glucose measurement of mice fasted for 8hrs. (**C**) Blood glucose measurements during glucose tolerance test (GTT). (**D**) Circulating blood insulin levels before and after glucose injection. Data indicate mean +/- s.e.m.; KO n=6, WT n=15 *: $p < 0.05$, **: $p < 0.01$,***: $p < 0.001$, ****: $p < 0.0001$ by one-way ANOVA

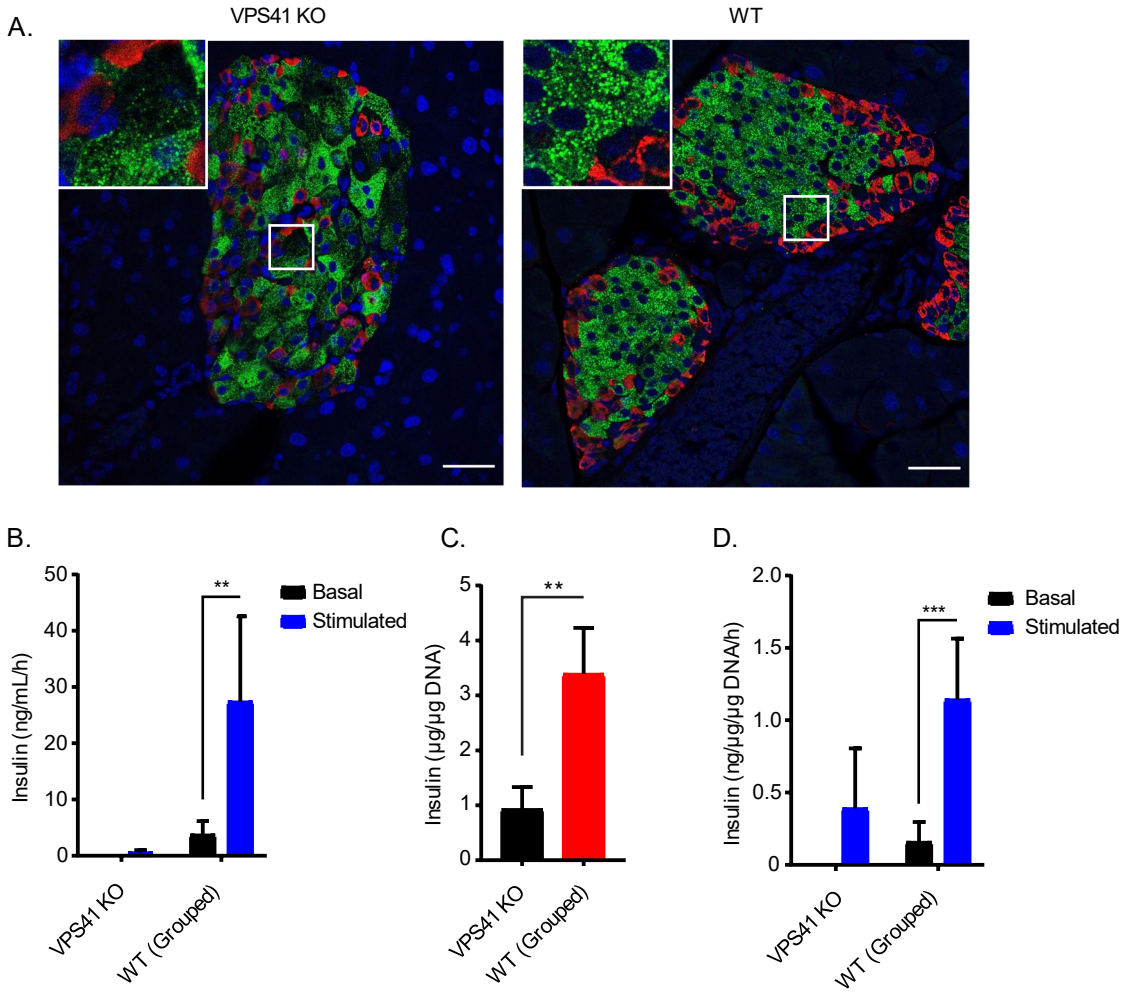

Figure 12: (**A**) Representative immunofluorescence images of whole pancreas slices from VPS41 KO and WT mice stained for insulin (green) and glucagon (red). Scale bar shows 100µm (**B**) Stimulated insulin secretion from isolated islets under basal or high glucose conditions. (**C**) Islet insulin content normalized to DNA content, analyzed by t-test. (**D**) Insulin secretion from isolated islets normalized to islet insulin concentration. Data indicate mean +/- s.e.m.; n=3 *: $p < 0.05$, **: $p < 0.01$,***: $p < 0.001$, ****: $p < 0.0001$ by one-way ANOVA

DISCUSSION

Loss of VPS41 from neuroendocrine PC12 cells and neurons leads to defects in peptidergic regulated secretion. SGs can still form, but they show altered size, and morphology (Asensio et al 2013). Consistent with this previous work, we now show that VPS41 is similarly required for insulin secretion. Thus, although SGs display a wide range of size and cargo content across specialized secretory cells, some of the molecular mechanisms controlling their formation seem conserved between neurons, neuroendocrine and endocrine cells.

The absence of VPS41 directly affects lysosomal function by disrupting HOPS function. This defect leads to an increase in lysosome and autophagosome biogenesis as demonstrated recently in non-secretory cells (van der Welle et al, unpublished). In agreement with this, we find that loss of VPS41 in INS-1 cells causes the expected defect in EGF degradation, together with a compensatory increase in active lysosomes and LC3 positive compartments. This effect seems to be mediated by mTORC1 inactivation leading to nuclear translocation of TFE3. This observation in conjunction with the decrease in cellular insulin stores raises the concern that pleiotropic effects associated with loss of HOPS might indirectly affect insulin secretion, for example by increasing insulin degradation. However, we have performed several key experiments to exclude this possibility. First, incubation of VPS41 KO INS-1 cells with lysosomal inhibitors did not change cellular insulin content, and insulin does not accumulate in late endosomes,

lysosomes or autophagosomes by immunofluorescence or by immuno-EM. In addition, pathways such as autophagy and crinophagy, which could potentially deliver SGs to the lysosome for degradation, are inherently HOPS-dependent processes (Jiang et al 2014, Csizmadia et al 2017). These observations thus exclude lysosomal degradation as a mechanism responsible for the defect in insulin storage in VPS41 KO cells. Second, KD of VPS39 leads to a similar defect in EGF degradation and LC3 accumulation, but these cells exhibit no change in insulin regulated secretion. This suggests that the effect of VPS41 is specific and independent of HOPS. Finally, the S285P human mutation, which is unable to rescue HOPS function, restores insulin secretion completely, indicating that it is actually possible to isolate HOPS dependent and independent functions of VPS41.

How does VPS41 mediate its effect on peptide hormone storage and regulated secretion? Although we can not yet determine the exact steps influenced by VPS41 during SG biogenesis, our data suggest that VPS41 controls sorting of transmembrane proteins, which ultimately might influence SG release properties. We have previously proposed that VPS41 could function at the TGN during budding of SGs (Asensio et al 2013) in neuroendocrine cells. Consistent with this, a pool of VPS41 localizes to the TGN (Pols et al 2013, Asensio et al 2013). Alternatively, VPS41 might be contributing to SG biogenesis by influencing maturation after budding. Interestingly, we have recently found that the large majority of newly-synthesized phogrin seems to be incorporated onto SG only after budding (Maslar et al, unpublished). Thus, it is tempting to speculate that retrograde pathways might contribute to SG maturation. Consistent with this, several cytosolic factors recently implicated in SG biogenesis seems to be typically associated

with the endocytic and retrograde pathways (Cattin-Ortola et al, unpublished, Topalidou et al, unpublished).

Consistent with recent studies in non-endocrine cells (Sharma et al 2019), we observed that VPS39 KD leads to degradation of VPS41. Interestingly, a pool of VPS41 remained stable, which raises the question of what confers the stability of this HOPS-independent pool of VPS41. It is tempting to speculate that post translational modifications (PTMs) such as phosphorylation are responsible. In yeast, VPS41 associates with two distinct compartments: AP-3 derived vesicles or the vacuole itself and this is mediated by phosphorylation of the membrane binding ALPS motif of VPS41 (Cabrera et al 2010). In mammalian cells, VPS41 phosphorylation by p38alpha-MAPK has been shown to regulate HOPS recruitment to vLPS compartments to mediate their fusion with the lysosome (Barry et al 2012). It will be interesting to test, in the future, whether phosphorylation or other yet to identify PTMs regulates VPS41 stability.

Interestingly, islets of BTBR mice, which are prone to develop diabetes, exhibit decreased levels of VPS41 gene expression (Keller et al 2008). In agreement with this, we now show that mice with a specific deletion of VPS41 in β-cells are overtly diabetic. Indeed, these animals display extreme fasting hyperglycemia and are glucose intolerant due to a defect in insulin secretion. Disruption of lysosome genes such as raptor (Ni et al 2017) leads to a very similar phenotype, however, in this case, the defect in secretion seems to be linked to β-cell maturation and early onset decreases in β-cell mass. In contrast, we observe no obvious difference in islet size and morphology in absence of VPS41. The mouse phenotype thus indicates that VPS41 plays a significant role for

glucose homeostasis and normal physiology. Furthermore, our observation that the human mutation S285P is able to rescue the regulated secretory defect of VPS41 KO cells but not HOPS-specific phenotypes helps explain why patients bearing this mutation have no observable endocrine associated defects. It might also provide a rationale to explain why these patients are alive, whereas VPS41 full KO mice die during early embryogenesis (Aoyama et al 2012). Altogether, our data emphasize the physiological significance of understanding the mechanism of SG formation at the molecular level. Unraveling the role of cytosolic factors in this process could help reveal potential therapeutic targets for the treatment of metabolic and endocrine associated diseases.

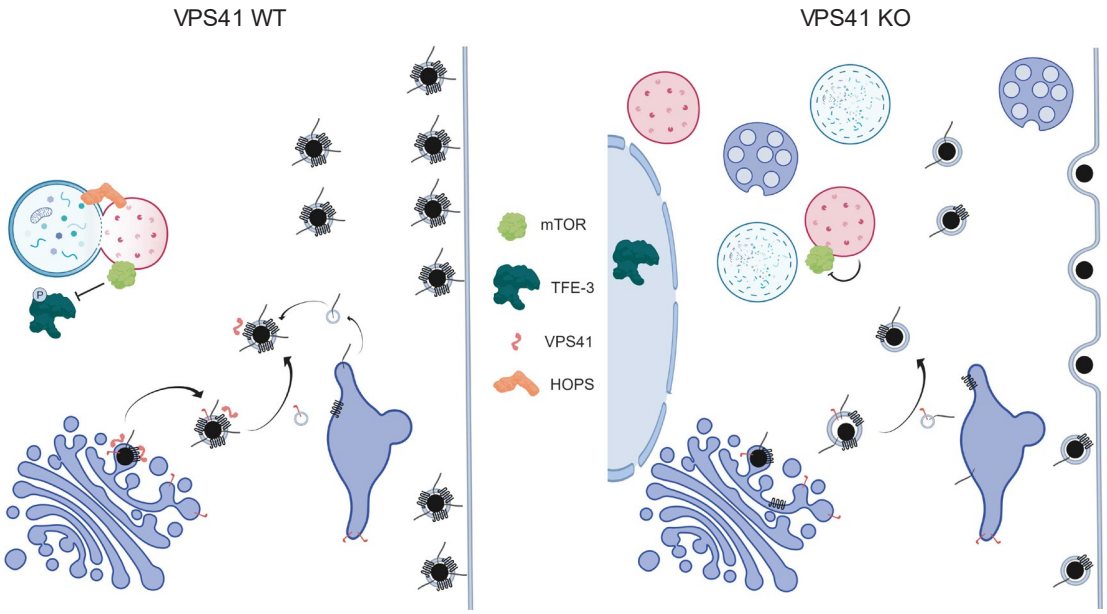

Figure 13: Model of VPS41 action in WT VPS41 (**left**) or VPS41 KO (**right**) cells. We propose that increased mis-sorting of transmembrane SG cargos leads to increased basal secretion events, which ultimately leads to downstream decreases in insulin storage as well as insulin SG release properties.

Given what we know, we propose a model (**Fig 13**) wherein VPS41 may be acting at both the TGN, either as a coat protein (Asensio et al 2013) or in some other capacity potentially in conjunction with AP3, or in the post-Golgi maturation of SGs, potentially in maintaining the transmembrane identity of these granules.

Although the exact mechanism of VPS41 action in regulated secretion has not been elucidated here, we have opened several new avenues of potential research in order to get at this very question. Future work will focus on identifying the mechanism by which VPS41 is able to exist outside of HOPS, potential interacting partners in the regulated pathway, and at which stage in biogenesis (budding or maturation) these factors are playing a role in. VPS41 is predicted to be potentially ubiquitinated (Ubpred) at both the N- and C-terminus where it has been shown to interact directly with AP3 (Asensio et al 2013) and the HOPS complex (Hunter et al 2017). Perhaps the mechanism regulating the entry of VPS41 in this pathway is which of these sites is accessible for ubiquitination. To address this, we can deplete VPS39 from cells expressing VPS41, and look for sites of ubiquitination, in addition to other PTMs, in proteasome defective (MG132) cells via mass spectrometry proteomics. To identify potential protein partners for VPS41 within the regulated secretory pathway, we would propose to do proximity labeling (Kim et al, 2016) of both WT VPS41 and the VPS41^{S284P} patient mutant in both KO and KO depleted of VPS39 cells. We would anticipate that the patient mutation could potentially aid in identifying novel SG associated interacting partners, but its ability to associate with HOPS still might limit its relevance in this context (van der Welle et al, unpublished). When we prevent HOPS association via KD or KO of VPS39, we anticipate being able to

narrow in on the factors aiding in its HOPS-independent functions. In addition to this, another potentially interesting avenue of work could be to identify residues and domains of VPS41 regulating its interactions with the HOPS complex, which may give more insight into how VPS41 is differentially regulated. This could be achieved by performing a yeast-2-hybrid screen with mutant alleles of VPS41 generated via random mutagenesis. Although this is not a trivial task, it could potentially provide much needed insight into the role of these different VPS41 domain in its many different functions. Finally, to identify which part of the pathway, budding or maturation, VPS41 is acting on, we are performing iEM of VPS41 in INS-1 cells to determine if VPS41 is localized to budding secretory granules at the TGN, post-Golgi SGs, or if it cannot be localized to either, suggesting a less directly mechanism of action. This could perhaps be improved upon, by increasing the relative pool of VPS41 that can effectively participate in this partway by KD or KO of VPS39. Overall the precise role of VPS41 in the regulated secretory pathway, and even outside of HOPS (Pols et al 2013), is still rife with opportunity and unexplored avenues of research. Advances in these mechanisms could help with targeted therapies to help treat patients suffering from defects in VPS41 and associated pathways.

REFERENCES

Ailion, Michael, et al. "Two Rab2 Interactors Regulate Dense-Core Vesicle Maturation." *Neuron* 82.1 (2014): 167-180.

Aoyama, Minako, et al. "Spatial Restriction of Bone Morphogenetic Protein Signaling in Mouse Gastrula through the mVam2-Dependent Endocytic Pathway." *Developmental Cell* 22.6 (2012): 1163-1175.

Arvan, P and D Castle. "Sorting and storage during secretory granule biogenesis: looking backward and looking forward." *The Biochemical journal* 332 (Pt 3).Pt 3 (1998): 593-610.

Asensio, Cédric S, Daniel W Sirkis and Robert H Edwards. "RNAi screen identifies a role for adaptor protein AP-3 in sorting to the regulated secretory pathway." *The Journal of cell biology* 191.6 (2010): 1173-87.

Asensio, Cédric S., et al. "Self-Assembly of VPS41 Promotes Sorting Required for Biogenesis of the Regulated Secretory Pathway." *Developmental Cell* 27.4 (2013): 425-437.

Balderhaar, Henning J kleine and Christian Ungermann. "CORVET and HOPS tethering complexes - coordinators of endosome and lysosome fusion." *Journal of cell science* 126.Pt 6 (2013): 1307-16.

Barry, Abdoulaye Oury, et al. "Impaired Stimulation of p38α-MAPK/Vps41-HOPS by LPS from Pathogenic Coxiella burnetii Prevents Trafficking to Microbicidal Phagolysosomes." *Cell Host & Microbe* 12.6 (2012): 751-763.

Boncompain, Gaelle, et al. "Synchronization of secretory protein traffic in populations of cells." *Nature Methods* 9.5 (2012): 493-498.

Cabrera, Margarita, et al. "Phosphorylation of a membrane curvature-sensing motif switches function of the HOPS subunit Vps41 in membrane tethering." *The Journal of cell biology* 191.4 (2010): 845-59.

Cao, Mian, et al. "PICK1 and ICA69 control insulin granule trafficking and their deficiencies lead to impaired glucose tolerance." *PLoS biology* 11.4 (2013): e1001541

Cattin-Ortolá, Jérôme, et al. "CCDC186 recruits EARP and controls dense-core vesicle cargo sorting by exit." *bioRxiv* (2019): 616458.

Cong, L., et al. "Multiplex Genome Engineering Using CRISPR/Cas Systems." *Science* 339.6121 (2013): 819-823.

Csizmadia, Tamás, et al. "Molecular mechanisms of developmentally programmed crinophagy in Drosophila." *The Journal of cell biology* 217.1 (2018): 361-374.

Dikeakos, Jimmy D and Timothy L Reudelhuber. "Sending proteins to dense core secretory granules: still a lot to sort out." *The Journal of cell biology* 177.2 (2007): 191-6.

Edwards, Stacey L., et al. "Impaired dense core vesicle maturation in Caenorhabditis elegans mutants lacking Rab2." *The Journal of Cell Biology* 186.6 (2009): 881-895.

Erlendsson, Simon, et al. "Protein interacting with C-kinase 1 (PICK1) binding promiscuity relies on unconventional PSD-95/discs-large/ZO-1 homology (PDZ) binding modes for nonclass II PDZ ligands." *The Journal of biological chemistry* 289.36 (2014): 25327-40.

Gehart, Helmuth, et al. "The BAR Domain Protein Arfaptin-1 Controls Secretory Granule Biogenesis at the trans-Golgi Network." *Developmental Cell* 23.4 (2012): 756-768.

Gerdes, H H, et al. "The primary structure of human secretogranin II, a widespread tyrosine-sulfated secretory granule protein that exhibits low pH- and calcium-induced aggregation." *The Journal of biological chemistry* 264.20 (1989): 12009-15.

Hannemann, M, et al. "TBC-8, a Putative RAB-2 GAP, Regulates Dense Core Vesicle Maturation in Caenorhabditis elegans." *PLoS Genet* 8.5 (2012): 1002722.

Henquin, J. C. "Triggering and amplifying pathways of regulation of insulin secretion by glucose." *Diabetes* 49.11 (2000): 1751-1760.

Hinners, Ina, et al. "AP-1 recruitment to VAMP4 is modulated by phosphorylation-dependent binding of PACS-1." *EMBO reports* 4.12 (2003): 1182-1189.

Holst, Birgitte, et al. "PICK1 Deficiency Impairs Secretory Vesicle Biogenesis and Leads to Growth Retardation and Decreased Glucose Tolerance." *PLoS Biology* 11.4 (2013): e1001542.

Hummer, Blake H, et al. "HID-1 controls formation of large dense core vesicles by influencing cargo sorting and trans-Golgi network acidification." *Molecular biology of the cell* 28.26 (2017): 3870-3880.

Hunter, Morag R, et al. "Proteomic and Biochemical Comparison of the Cellular Interaction Partners of Human VPS33A and VPS33B." *Journal of molecular biology* 430.14 (2018): 2153-2163.

Hunter, Morag R., et al. "VPS18 recruits VPS41 to the human HOPS complex via a RING–RING interaction." *Biochemical Journal* 474.21 (2017): 3615-3626.

Jaqaman, Khuloud, et al. "Robust single-particle tracking in live-cell time-lapse sequences." *Nature Methods* 5.8 (2008): 695-702.

Jiang, Peidu, et al. "The HOPS complex mediates autophagosome-lysosome fusion through interaction with syntaxin 17." *Molecular biology of the cell* 25.8 (2014): 1327-37.

Jonker, C. T. H., et al. "Vps3 and Vps8 control integrin trafficking from early to recycling endosomes and regulate integrin-dependent functions." *Nature Communications* 9.1 (2018): 792.

Keller, M. P., et al. "A gene expression network model of type 2 diabetes links cell cycle regulation in islets with diabetes susceptibility." *Genome Research* 18.5 (2008): 706-716.

Klumperman, J, et al. "Mannose 6-phosphate receptors are sorted from immature secretory granules via adaptor protein AP-1, clathrin, and syntaxin 6-positive vesicles." *The Journal of cell biology* 141.2 (1998): 359-71.

Maslar, D., et al. "Synchronization of regulated secretory cargo trafficking in neuroendocrine cells reveals differential trans-Golgi network budding behavior for soluble and transmembrane proteins" Unpublished (2019)

Nakamura, N, et al. "Vam2/Vps41p and Vam6/Vps39p are components of a protein complex on the vacuolar membranes and involved in the vacuolar assembly in the yeast Saccharomyces cerevisiae." *The Journal of biological chemistry* 272.17 (1997): 11344-9.

Natori, S. and W. B. Huttner. "Chromogranin B (secretogranin I) promotes sorting to the regulated secretory pathway of processing intermediates derived from a peptide hormone precursor." *Proceedings of the National Academy of Sciences* 93.9 (1996): 4431-4436.

N'Diaye, Elsa-Noah, et al. "PLIC proteins or ubiquilins regulate autophagy-dependent cell survival during nutrient starvation." *EMBO reports* 10.2 (2009): 173-179.

Ni, Qicheng, et al. "Raptor regulates functional maturation of murine beta cells." *Nature communications* 8 (2017): 15755.

Orci, L, et al. "Proteolytic maturation of insulin is a post-Golgi event which occurs in acidifying clathrin-coated secretory vesicles." *Cell* 49.6 (1987): 865-8.

Pinheiro, Paulo S, et al. "The BAR domain protein PICK1 controls vesicle number and size in adrenal chromaffin cells." *The Journal of neuroscience : the official journal of the Society for Neuroscience* 34.32 (2014): 10688-700.

Pols, Maaike S., et al. "hVps41 and VAMP7 function in direct TGN to late endosome transport of lysosomal membrane proteins." *Nature Communications* 4.1 (2013): 1361.

Pols, S., et al. "The HOPS Proteins hVps41 and hVps39 Are Required for Homotypic and Heterotypic Late Endosome Fusion." *Traffic* 14.2 (2013): 219-232.

Puertollano, Rosa. "mTOR and lysosome regulation." *F1000prime reports* 6 (2014): 52.

Resa, Te, Lynn Burgess and Regis B Kelly. "CONSTITUTIVE AND REGULATED SECRETION OF PROTEINS." 1987.

Sasidharan, Nikhil, et al. "RAB-5 and RAB-10 cooperate to regulate neuropeptide release in Caenorhabditis elegans." *Proceedings of the National Academy of Sciences of the United States of America* 109.46 (2012): 18944-9.

Sumakovic, Marija, et al. "UNC-108/RAB-2 and its effector RIC-19 are involved in dense core vesicle maturation in Caenorhabditis elegans." *The Journal of cell biology* 186.6 (2009): 897-914.

Thiele, C, H H Gerdes and W B Huttner. "Protein secretion: puzzling receptors." *Current biology : CB* 7.8 (1997): R496-500.

Thorens, Bernard, et al. "Ins1 Cre knock-in mice for beta cell-specific gene recombination." *Diabetologia* 58.3 (2015): 558-565.

Tooze, Sharon A. "Biogenesis of secretory granules in the trans-Golgi network of neuroendocrine and endocrine cells." *Biochimica et Biophysica Acta (BBA) - Molecular Cell Research* 1404.1-2 (1998): 231-244.

Topalidou, Irini, Jérôme Cattin-Ortolá and Michael Ailion. "EIPR1 controls dense-core vesicle cargo sorting and EARP complex localization in insulinoma cells." *bioRxiv* (2018): 374488.

van der Beek, Jan, et al. "CORVET, CHEVI and HOPS - multisubunit tethers of the endo-lysosomal system in health and disease." *Journal of cell science* 132.10 (2019): jcs189134.

van der Welle, Reini, et al. "Heterozygous expression of VPS41 variants cause a neurological disorder by inhibiting HOPS function and mTORC1 Signaling" Unpublished (2019)

Varadi, Aniko, et al. "Kinesin I and cytoplasmic dynein orchestrate glucose-stimulated insulin-containing vesicle movements in clonal MIN6 β-cells." *Biochemical and Biophysical Research Communications* 311.2 (2003): 272-282.

Xu, H. and D Shields. "Prohormone processing in the trans-Golgi network: endoproteolytic cleavage of prosomatostatin and formation of nascent secretory vesicles in permeabilized cells." *The Journal of Cell Biology* 122.6 (1993): 1169-1184.

Zhang, Xu, Lan Bao and Guo-Qiang Ma. "Sorting of neuropeptides and neuropeptide receptors into secretory pathways." *Progress in Neurobiology* 90.2 (2010): 276-283.

APPENDIX: Supplemental Figures

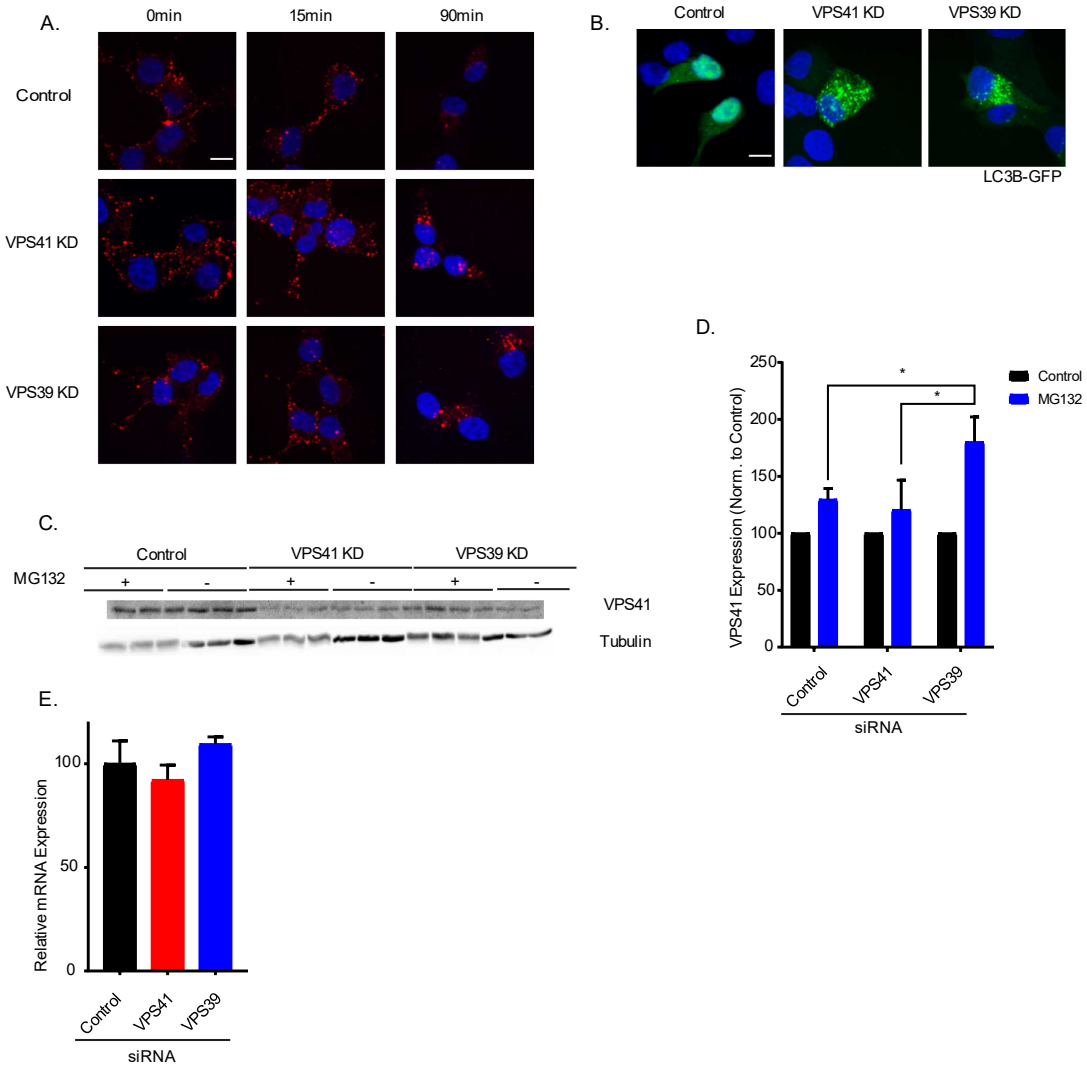

Figure S1: (**A**) Representative images of EGF-647 labeled cells before or after a short (15min) or long (90min) chase. (**B**) Representative images of cells co-transfected with indicated siRNAs and LC3-eGFP. (**C**) siRNA treated cells incubated with 5μM MG132 or DMSO for 12 hr prior to lysis and western blot analysis for VPS41 and tubulin. VPS41 levels were normalized to tubulin expression and quantified (**D**) in comparison to their respective controls (**E**) qPCR analysis of insulin RNA levels. n=3 *: $p < 0.05$ by one-way ANOVA

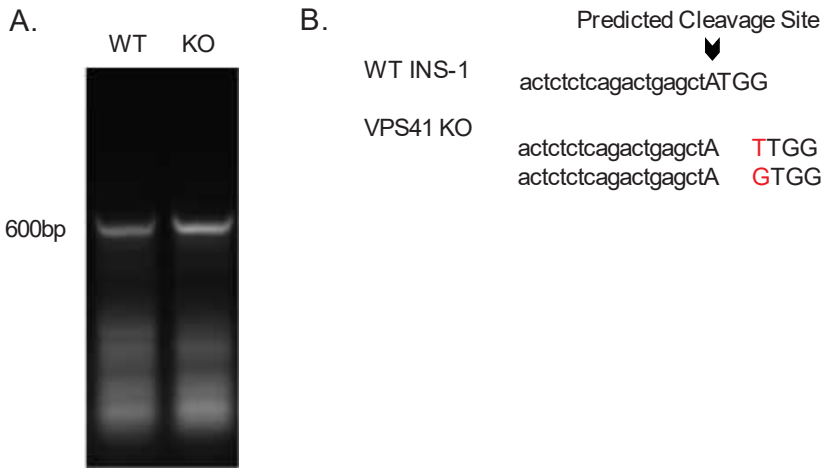

Figure S2: (**A**) PCRs from genomic DNA isolated from WT and VPS41 KO INS-1 cells show a band at 600bp representing sequence surrounding exon 1 of the rat VPS41 sequence. (**B**) RNA guide sequence and predicted cleavage site for Cas9. Indels, both single base pair insertions, are shown in red in sequence disrupting the initiator ATG in Exon 1.

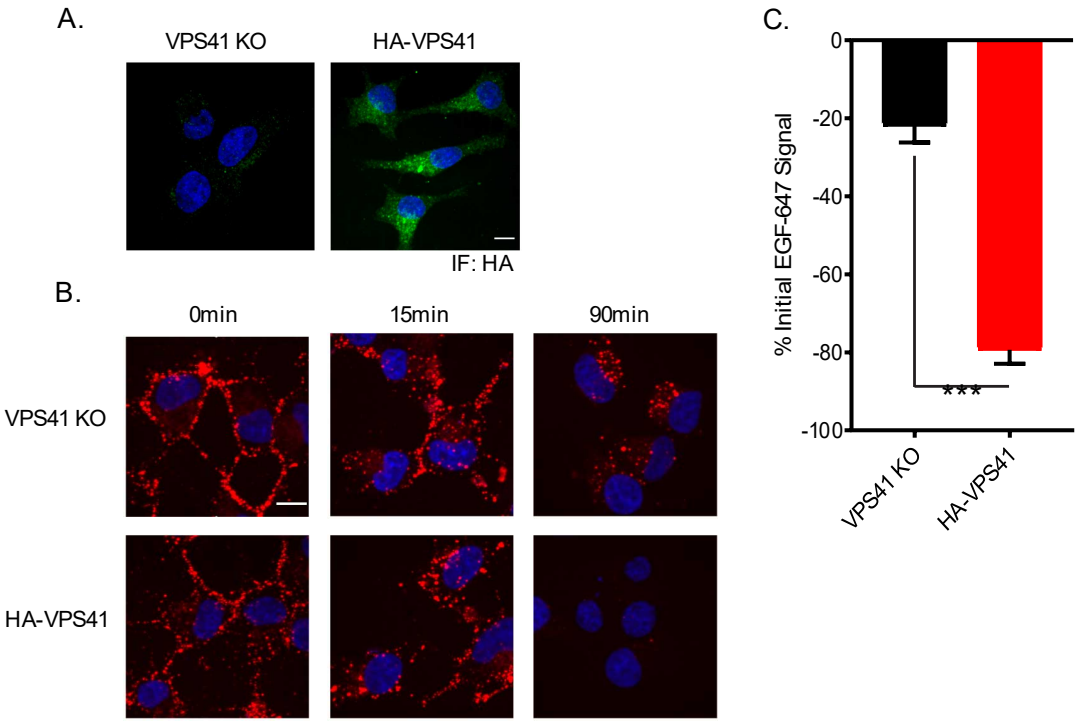

Figure S3: (**A**) Representative images of VPS41 KO and HA-VPS41 rescue INS-1 cells stained for HA. (**B**) Representative images of EGF-647 labeled cells before or after a short (15min) or long (90min) chase. (**C**) Quantification of the change in EGF-647 fluorescence between 0 min and 90 min. Data indicate mean +/- s.e.m.; n=3 ***: $p < 0.001$ Scale bars indicate 10 μm.

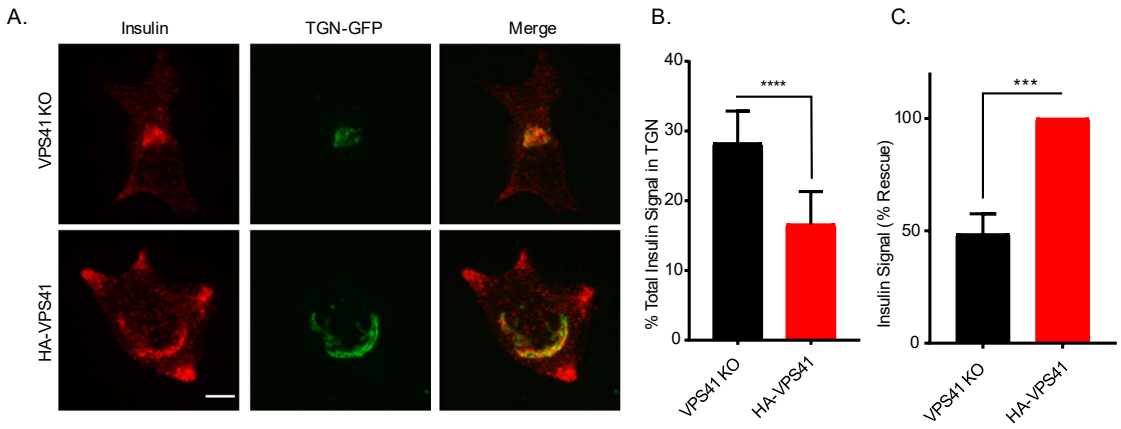

Figure S4: (**A**) Representative images of INS-1 VPS41 KO or HA-VPS41 cells transfected with TGN-eGFP and stained for insulin. (**B**) Percentage of total insulin fluorescent signal localized within the masked Golgi region. (**C**) Total insulin immunoreactive fluorescent signal in VPS41 KO cells normalized to insulin signal in the HA-VPS41 rescue. Data indicate mean +/- s.e.m.; n=3 ***: $p < 0.001$, ****: $p< 0.0001$. Scale bars indicate 10 µm.

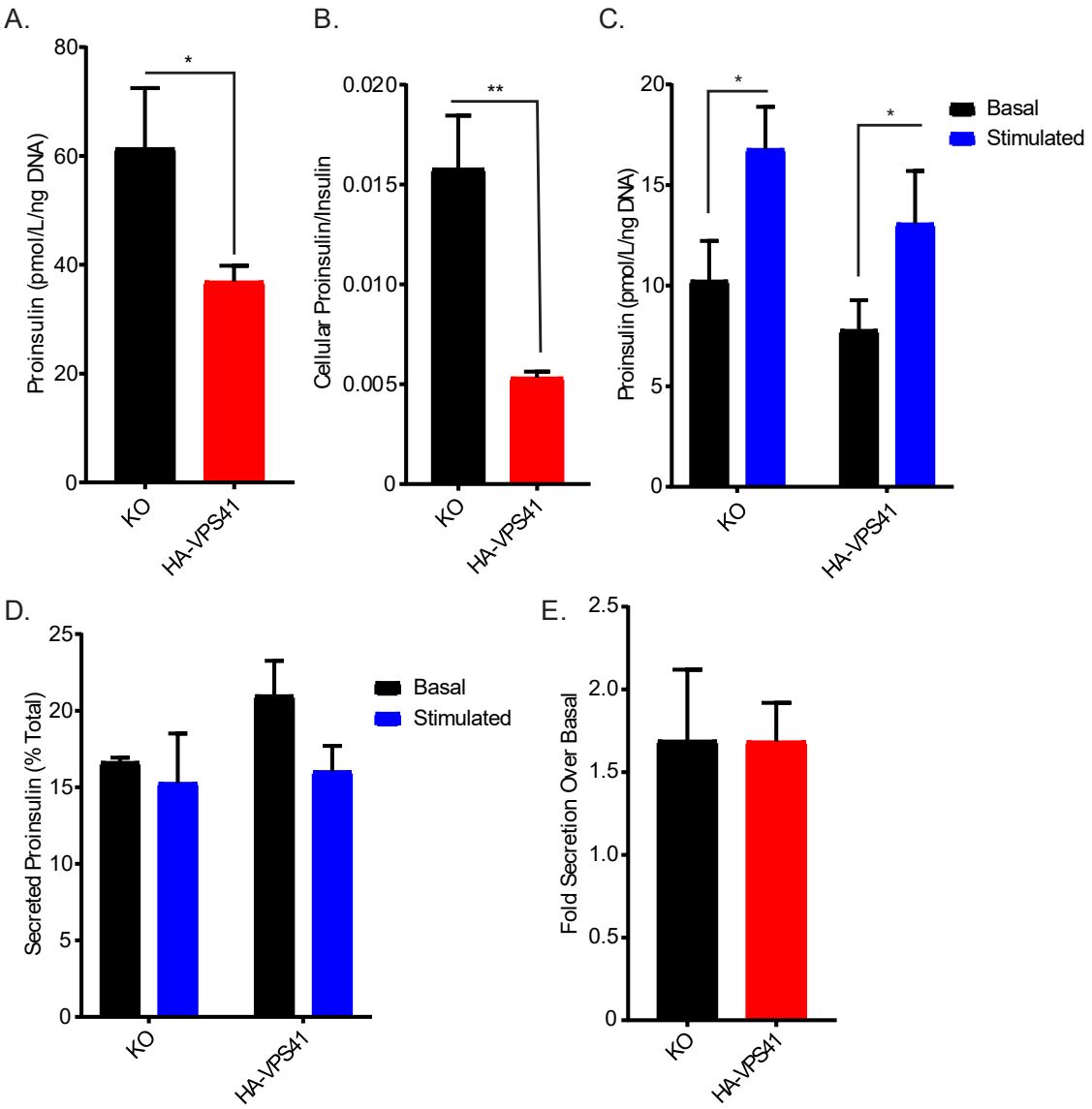

Figure S5: (**A**) Total cellular proinsulin pool under basal conditions. (**B**) Total cellular ratio of proinsulin:insulin under basal conditions. (**C**) Basal and stimulated proinsulin release from VPS41 KO and rescue INS-1, analyzed by ANOVA. (**D**) Basal and stimulated proinsulin release from VPS41 KO and rescue INS-1 normalized to total cellular stores, analyzed by ANOVA. (**E**) Proinsulin secretion, fold stimulated release over basal release. Data indicate mean +/- s.e.m.; n=3 *: $P < 0.05$, **: $P < 0.01$ by t-test

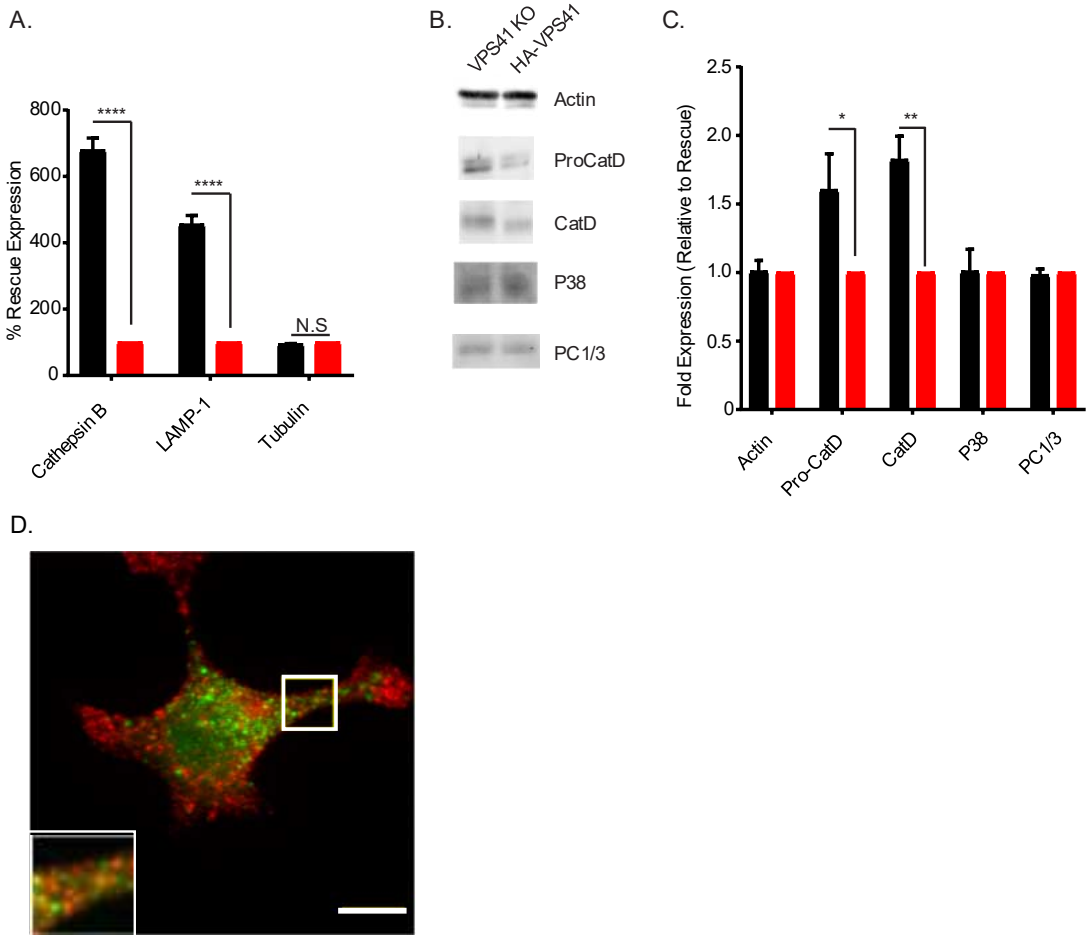

Figure S6: (**A**) Level of expression of lysosomal gene products by qPCR of lysosomal genes (LAMP-1 and Cathepsin B). (**B**) Lysates from VPS41 KO and HA-VPS41 rescue INS-1 cells were immunoblotted using antibodies directed against the indicated proteins and quantified (**C**) and normalized to expression in the HA-VPS41 lysate. (**D**) Representative image of VPS41 KO cells stained for insulin after transfection with LC3-GFP. Scale bars indicate 10 μm. Data indicate mean +/- s.e.m.; n=3 *: $P < 0.05$, **: $P < 0.01$, ****: $P < 0.0001$

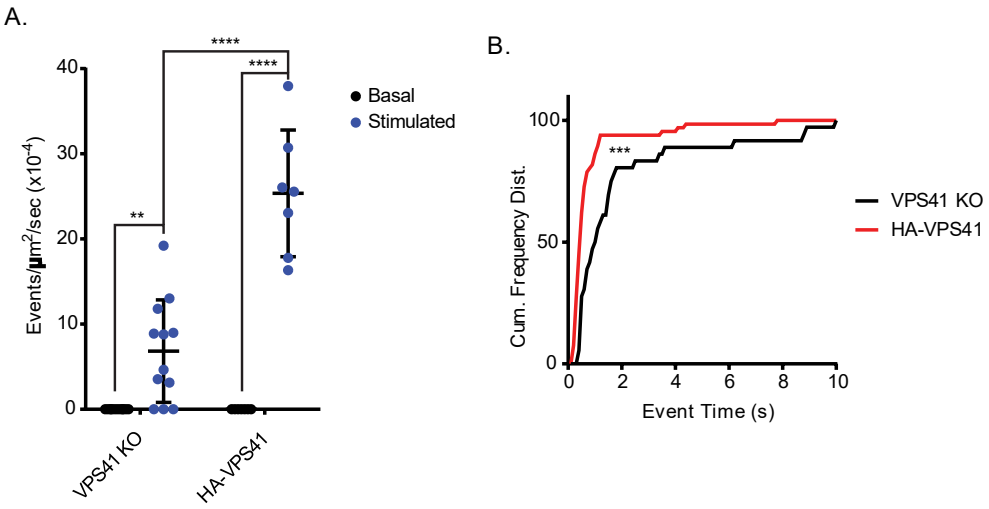

Figure S7: (**A**) Quantification of NPY-pHluorin exocytosis events in VPS41 KO and HA-VPS41 rescue INS-1 cells over a 10s basal or stimulated period 3hrs post-biotin addition. (**B**) Cumulative frequency distribution of NPY-pHluorin exocytosis event duration in VPS41 KO and rescue cells. .Data indicate mean +/- s.e.m.; n=3 *: ***: $p < 0.001$, ****: $p < 0.0001$ Event number analyzed by one-way ANOVA. Event duration analyzed by Kolmogorov Smirnov.

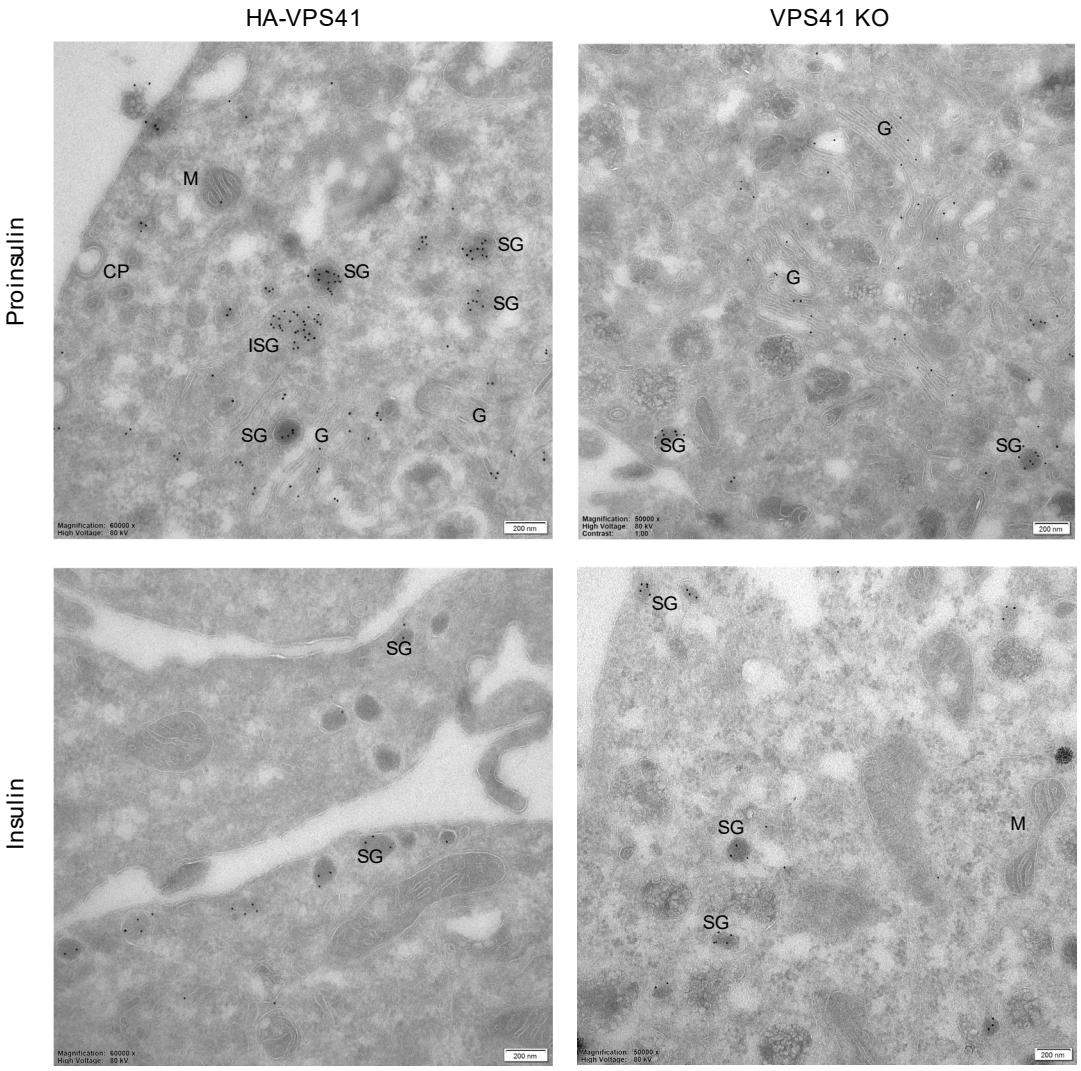

Figure S8: Representative images of VPS41 KO and HA-VPS41 cells stained for proinsulin and insulin with gold labeled antibodies.

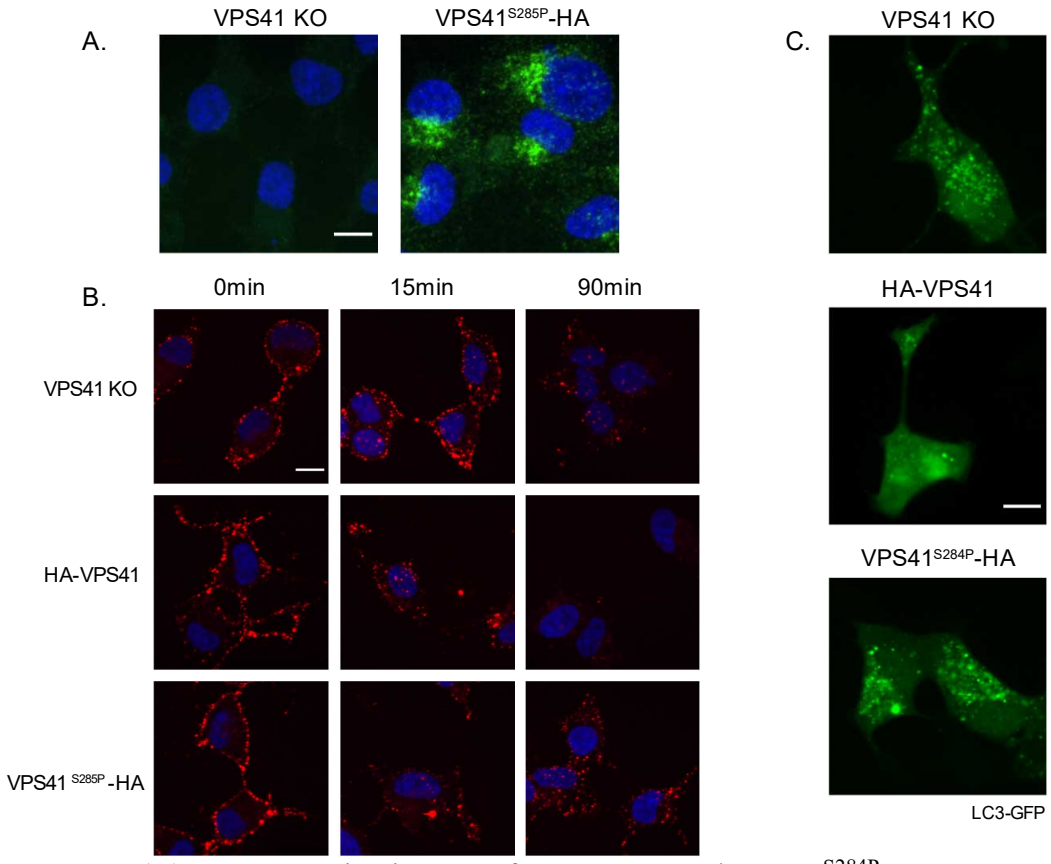

Figure S9: (**A**) Representative images of VPS41 KO and VPS41^{S284P}-HA INS-1 rescue cells stained for HA. (**B**) Representative images of EGF-647 labeled cells before or after a short (15 min) or long (90 min) chase. (**C**) Representative images of INS-1 cells transfected with LC3-eGFP. Scale bars indicate 10μm.

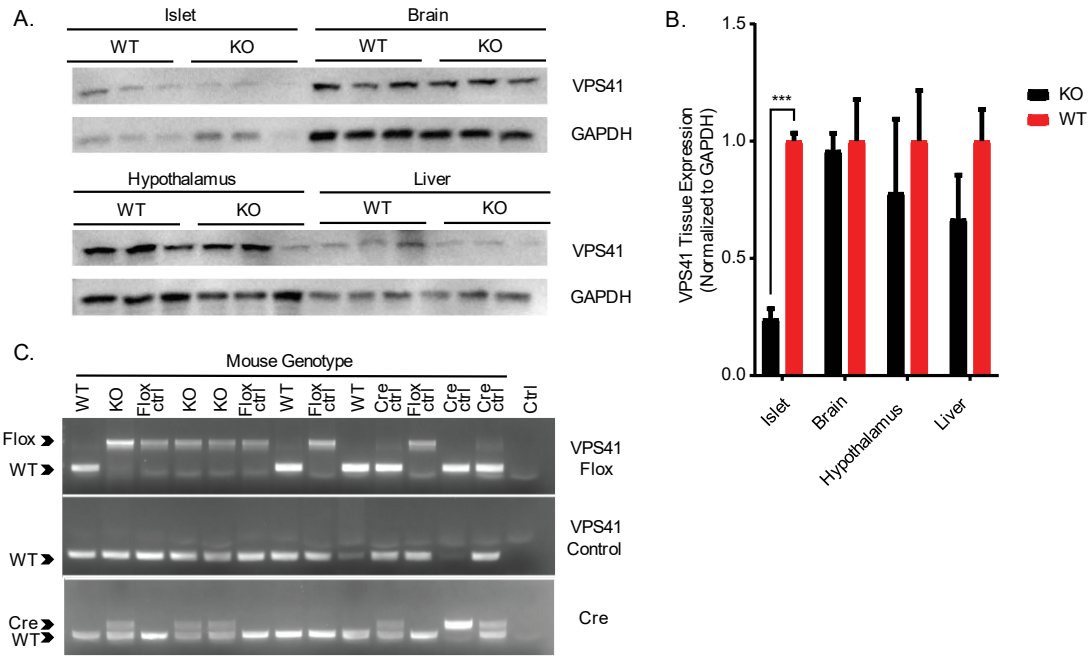

Figure S10: (**A**) Representative western blots of VPS41 protein levels in various tissues from 15 week old age-matched WT or VPS41 KO mice. (**B**) GAPDH normalized tissue VPS41 protein expression levels. (**C**) Representative gels of mouse genotyping

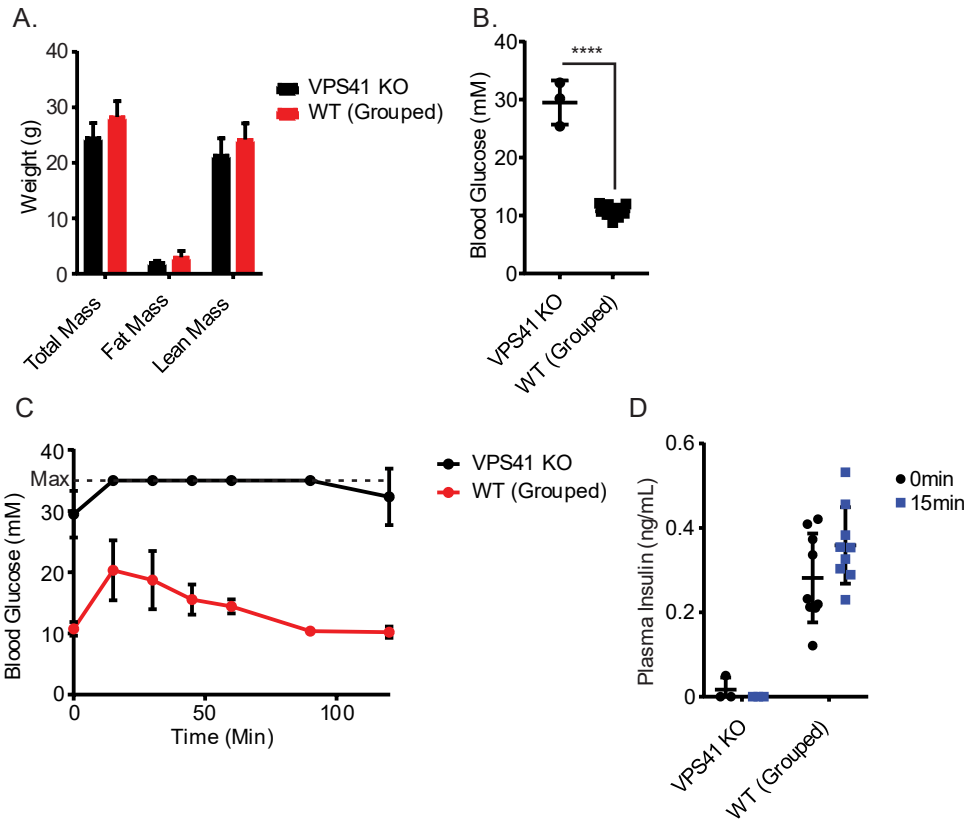

Figure S11: (**A**) Fat and lean mass measurements of age matched 15 week old WT and VPS41 KO mice. (**B**) Blood glucose measurement of mice fasted for 8hrs. (**C**) Blood glucose measurements during glucose tolerance test (GTT) (**D**) Circulating blood insulin levels before and after glucose injection. Data indicate mean +/- s.e.m.; KO n=3, WT n=9 *: $p < 0.05$, **: $p < 0.01$,***: $p < 0.001$, ****: $p < 0.0001$ by one-way ANOVA

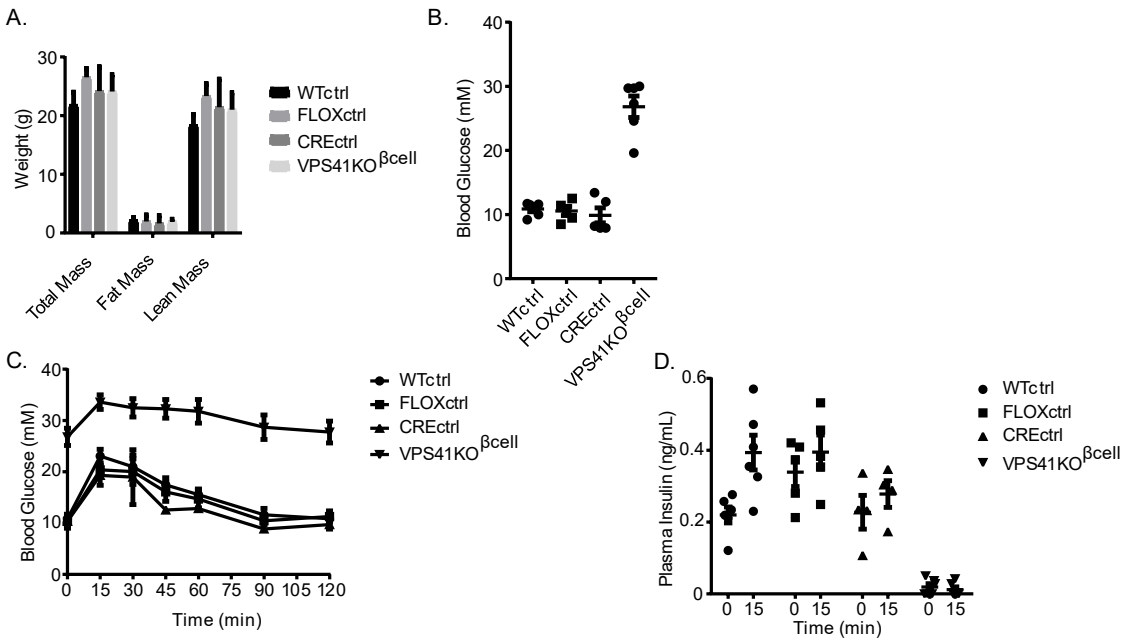

Figure S12: (**A**) Fat and lean mass measurements of age matched 8 week old WT, Cre control, Vam2 fl/fl control, and VPS41 KO mice. (**B**) Blood glucose measurement of mice fasted for 8hrs. (**C**) Blood glucose measurements during glucose tolerance test (GTT) (**D**) Circulating blood insulin levels before and after glucose injection. Data indicate mean +/- s.e.m.; KO n=6, WT n=15 *: $p < 0.05$, **: $p < 0.01$,***: $p < 0.001$, ****: $p < 0.0001$ by one-way ANOVA